Measurements of the Electromagnetic Properties of Some Microwave-Absorbing Materials

W. Hartung, D. Moffat, & T. Hays

13 January 1993

1 Introduction

Present plans for CESR-B, the proposed upgrade of CESR into a B factory, call for 16 single-cell B-band (500 MHz fundamental) superconducting accelerating cavities. Estimates suggest that the loaded Q of all the dangerous higher-order modes of the cavity must be less than 100 in order to ensure beam stability with the many stored bunches required for CESR-B. To damp the modes to this degree, a large beam tube diameter is to be used, thus allowing (almost) all of the higher-order modes to propagate into the beam tube. A layer of dissipative material on the inside surface of the beam tube is to absorb the electromagnetic fields that propagate into the tube and thereby provide the mode damping. This is done a safe distance away from the cavity so that the fundamental (accelerating) mode is not affected and the power is dissipated at room temperature. Because the material is on the inner surface of the beam tube, it can also interact directly with the passing beam. The load material and geometry must permit the load to strongly damp cavity modes, but must prevent the load from harming the beam or being harmed by the beam.

Several commercially-available microwave-absorbing materials are being considered for the load. Room-temperature measurements on a full-scale copper model of the cavity with loads made from two possible absorbing materials, ferrite-50 and TT2-111-series ferrite, have demonstrated that the cavity higher-order modes can be damped effectively with either of these materials [1]. To help us choose from the many possible materials, we would like to predict the higher-order mode damping ability of a given material. We would also like to predict how a load made from a given material interacts with the beam. Such predictions require knowledge of the microwave properties of the material; for the most part, however, the microwave properties are not known over the relevant frequency range. It was decided, therefore, to measure the microwave properties of some of the more promising materials. Seven potential B factory load materials have been measured; one other material of interest to our colleagues at CEBAF (perhaps applicable to B factory use also) has also been measured. Further measurements on some dielectric materials with known microwave properties were done to check our measurement and analysis techniques.

All of the materials were assumed to be linear (in their response to electric and magnetic fields), homogeneous and isotropic. Under these assumptions, the microwave properties may be described by a complex magnetic permeability and complex electric permittivity. Since the materials are assumed isotropic, the permeability and permittivity are scalars, rather than tensors. The permeability and permittivity were measured using the coaxial transmission line technique [2]. The preliminary results are reported herein. Attempting to characterise these materials was a learning experience for us, which is why interim results for the first material we measured (ferrite-50), which have been reported earlier [3, 4, 5], differ significantly from those presented here.

In this note, we will first review the salient points of the theory of the transmission line measurement method, paying particular attention to sign and phase ambiguities. We will then discuss the experimental methods we used, which, aside from our technique for ensuring good contact between the sample and host air line, match the established methods quite closely. We will next turn to our analysis procedures, explaining why we used a different method for resolving the phase ambiguities and discussing measurement errors. We will then present the results of our measurements and a few interpretations of them. Finally, we will describe a simple modification to the analysis procedure, applicable for materials with known ϵ or known μ, which may be used to avoid some of the difficulties with the usual analysis.

2 A Review of the Theory of the Measurements

To facilitate subsequent discussion, the highlights of the theory underlying the measurement technique will now be reviewed. More detailed derivations may be found in the literature [2, 6, 7]. We will accord a bit more attention to sign ambiguities than is the norm. The basic strategy of the measurement is to fill part of a transmission line with the material, measure the reflection and transmission coefficients for the frequencies of interest, and thence deduce the permeability μ and permittivity ϵ.

Consider a travelling wave propagating through a TEM transmission line. The transmission line of interest is coaxial, although this discussion will apply to any TEM line. We assume that the voltage V, current I, fields, *etc.* are the real parts of complex quantities. Because of the Great Sign Ambiguity which arises from the introduction of complex quantities[1], we must choose a sign convention. We will suppose that the time dependence in V and I is given by $e^{i\omega t}$, ω being the angular frequency, a convenient choice as it is the one made by our network analysers. The reader should not conclude that this sign convention is used universally. By choosing the opposite sign convention, as some authors do, we would end up with μ and ϵ values that are the complex conjugates of those obtained with the $e^{i\omega t}$ convention (it has been asserted that one of these sign conventions is the physicist's convention and the other is the electrical engineer's, but we will not make such a seditious claim). We can only recommend that the reader exercise caution when dealing with complex μ and ϵ values, because the signs of the imaginary parts of μ and ϵ are meaningful, in spite of their ambi-

[1] for readers who are unfamiliar with complex numbers, the Great Sign Ambiguity stems from the fact that the equation $x^2 = -1$ has two solutions which differ in sign but are otherwise indistinguishable.

guity: with our sign convention, we expect the imaginary parts of μ and ϵ to be negative in microwave-absorbing materials; positive values would correspond to "microwave-producing" materials.

In general, V and I must satisfy the wave equation, for which the general solution can be written

$$V(z,t) = V_1 e^{i(\omega t - k_z z)} + V_2 e^{i(\omega t + k_z z)}, \tag{1}$$

where k_z is the complex propagation wavenumber and V_1 and V_2 are complex amplitudes (a similar equation applies for $I(z,t)$). When Re $k_z > 0$, the first term in equation (1) corresponds to a forward-going wave (travelling in the $+z$ direction) and the second term corresponds to a reverse-going wave (travelling in the $-z$ direction). The transmission line has (complex) characteristic impedance Z.

Suppose that part of our transmission line is filled with a material characterised by a complex permittivity ϵ and complex permeability μ, while other parts of the line are filled with vacuum (we will use "vacuum" and "air" interchangeably, since the differences in their microwave properties are negligible at the level of precision of our measurements). In the material-filled part, we will have

$$k_z = \pm\omega\sqrt{\mu\epsilon} \tag{2}$$

$$Z = \pm\sqrt{\frac{\mu}{\epsilon}}\frac{Z_0}{Z_i}, \tag{3}$$

where Z_0 is the characteristic impedance of the vacuum-filled line and $Z_i = \sqrt{\mu_0/\epsilon_0}$. The sign ambiguities in k_z and Z reflect the fact that both forward-going and reverse-going waves are possible. The signs of k_z and Z are not independent, because they must satisfy

$$k_z Z = \omega\mu. \tag{4}$$

A sensible sign choice is the one which gives Re $k_z > 0$.

Let us consider first the case in which our transmission line is filled with material throughout its length. For a wave travelling in the forward direction, the complex ratio of the voltage at the $z = 0$ plane to the voltage at a plane $z = d$ plane (the "transmission coefficient" for a length d of filled line) is

$$T = e^{-ik_z d}. \tag{5}$$

Suppose next that our transmission line is filled with vacuum on the left and material on the right, with a transition at $z = 0$ (figure 1a). A forward-travelling wave incident from the vacuum side produces a reverse-going reflected wave and a forward-going transmitted wave. At the $z = 0$ plane, the complex ratio of the reverse voltage to the forward voltage (the "reflection coefficient" for the vacuum-material interface) is

$$\Gamma = \frac{Z - Z_0}{Z + Z_0}. \tag{6}$$

in terms of characteristic impedances. We can expect that $|\Gamma| \leq 1$ if our waves are travelling in the directions shown in figure 1a. Changing the sign of k_z and Z changes Γ and T to $1/\Gamma$ and $1/T$, respectively, which corresponds to waves travelling in directions that are opposite to those shown in figure 1a.

Now suppose that our transmission line is filled with material between the $z = 0$ plane and the $z = d$ plane, with vacuum on either side (figure 1b). With a forward-travelling wave incident from the left, there will be a reverse-travelling reflected wave on the left, a forward-travelling transmitted wave on the right, and waves travelling in both directions inside the material. The reflection coefficient at the $z = 0$ plane is

$$S_{11} = \frac{\Gamma(1 - T^2)}{1 - \Gamma^2 T^2}. \tag{7}$$

The transmission coefficient from the $d = 0$ plane to the $z = d$ plane is

$$S_{21} = \frac{T(1 - \Gamma^2)}{1 - \Gamma^2 T^2}. \tag{8}$$

Note that S_{11} and Γ are both reflection coefficients, but S_{11} refers to a line that is filled with material only between $z = 0$ and $z = d$, while Γ refers to a line filled with material for $z \geq 0$. Similarly, S_{21} refers to a line filled with material between $z = 0$ and $z = d$ only, while T refers to a line filled with material for all z.

The above results allow us to predict the reflection and transmission coefficients for a line with a material of known μ and ϵ. The quantities we can measure are S_{11} and S_{21} and the quantities we seek are μ and ϵ, so we need to retrace our steps. Solving equations (7) and (8) for T and Γ in terms of the S-parameters, we get

$$\Gamma = \chi \pm \sqrt{\chi^2 - 1} \tag{9}$$

$$T = \frac{S_{11} + S_{21} - \Gamma}{1 - (S_{11} + S_{21})\Gamma}, \tag{10}$$

where

$$\chi = \frac{S_{11}^2 - S_{21}^2 + 1}{2S_{11}}. \tag{11}$$

The sign ambiguity in the expression for Γ is such that if one choice of sign gives Γ and T, then the other choice of sign gives $1/\Gamma$ and $1/T$. Solving equations (5) and (6) for k_z and Z, we get

$$k_z = \frac{i}{d}\ln(T) \tag{12}$$

$$Z = Z_0\frac{1 + \Gamma}{1 - \Gamma}. \tag{13}$$

Equations (12) and (13) show that the ambiguity between Γ and T versus $1/\Gamma$ and $1/T$ produces an ambiguity between k_z and Z versus $-k_z$ and $-Z$, the same sign ambiguity we encountered earlier. Solving equations (2) and (3) for μ and ϵ, we get

$$\mu = \frac{k_z Z}{\omega} = \frac{k_z Z_0}{\omega}\frac{1 + \Gamma}{1 - \Gamma} \tag{14}$$

$$\epsilon = \frac{k_z}{Z\omega} = \frac{k_z}{Z_0\omega}\frac{1 - \Gamma}{1 + \Gamma}. \tag{15}$$

(a)

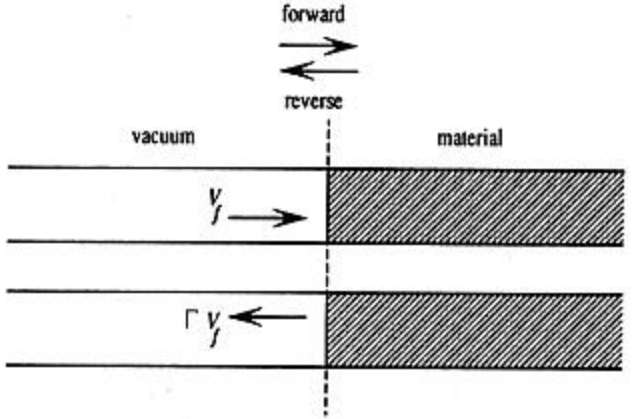

(b)

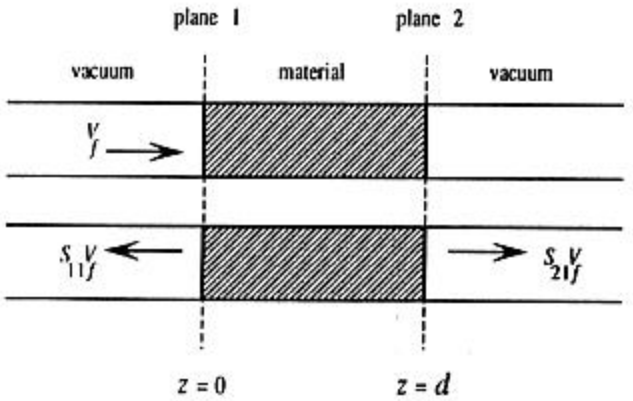

Figure 1. (a) A transmission line filled with vacuum on one side and a material with permeability μ and permittivity ϵ on the other side. (b) A transmission line filled with a length d of material with vacuum on both sides. A *TEM* wave with complex amplitude V_f is incident from the left; the phases of the waves are measured relative to the reference planes (dashed lines).

Because equations (14) and (15) for μ and ϵ involve only the product and the ratio of k_z and Z, $-k_z$ and $-Z$ give us the same μ and ϵ as k_z and Z, so, ultimately, our choice of sign in equation (9) does not matter. In the analysis, it is convenient to choose the case for which $|\Gamma| < 1$, which should give Re $k_z > 0$. Equations (14) and (15) allow us to determine the signs of the real and imaginary parts of μ and ϵ unambiguously.

There is another ambiguity in the analysis which arises from the complex logarithm in equation (12). The imaginary part of $\ln(T)$ is the phase of T, which is ambiguous by integer multiples of 2π. Physically, this ambiguity stems from the fact that Re $k_z d$ is the change in the phase of a forward-going wave as it travels through the length d of the material; knowing only the complex transmission coefficient T, we cannot deduce the total phase change without knowing the number of whole wavelengths that exist in the length d. We can write

$$k_z d = 2\pi n + \mathcal{PV}(k_z d), \tag{16}$$

where $\mathcal{PV}(k_z d)$ is the "principal value" of $k_z d$, which we define as the value of $k_z d$ whose real part is between 0 and 2π, and n is an integer. Because we chose our sign in equation (9) so that we should have Re $k_z > 0$, we can expect that $n \geq 0$. The integer n is equal to number of whole wavelengths that fit in the length d. We can obtain $\mathcal{PV}(k_z d)$ directly from T, but we cannot determine $k_z d$ directly, a problem we discuss in section 4.1.

3 Experimental Techniques

Samples of the material to be measured were machined into cylindrical "beads" to fit into the coaxial line. In the case of absorbing materials (all of which are ceramics), slabs of the material were first diamond core drilled to the approximate outer and inner diameter. The final diameter was ground on the outside and hand reamed on the inside (using a solid or expansion diamond reamer). The samples were cut to their final length with a slow-speed diamond saw. The chip from the saw cut was touched up using a hand-held grinding tool. Finally, samples were degreased in an acetone solution with ultrasonic agitation. The dielectric materials were machined with conventional techniques.

The samples were placed inside a standard 7 mm coaxial air line (inner conductor diameter 3.04 mm, outer diameter 7 mm, characteristic vacuum impedance $Z_0 = 50\ \Omega$) for the measurements. Initially, air lines with female type N connectors were used; precision 7 mm connectors were found to give less systematic error, however, so most of the measurements were done with the latter. Both commercially manufactured air lines and custom-made air lines were used. The custom-made lines with 7 mm connectors were made from brass rod with non-retractable sleeves on the outer conductor and spring-loaded centering pins on the inner conductor.

The first samples were not made with especially tight tolerances on the inner and outer diameters, so that most samples fit loosely in the air line. The next few samples were made with better tolerances to ensure a snug fit between the sample and the air line in an effort to improve the reproducibility of the measurements. For later samples, the tolerances were relaxed a little bit, but liquid metal was used to fill the air gaps between the sample and

air line with the aim of further improving the reproducibility. All of the measurements on absorbing materials covered herein were made with liquid metal in custom-made air lines, except for some of the comparative measurements discussed in section 6.3. The liquid metal was an alloy of gallium and indium, which has a melting point of 16°C at the eutectic composition. Filling the gaps between the sample and the air line without coating the faces of the sample with metal or leaving drops of liquid metal in the air line proved to be a difficult technique to master. With practice, our success rate with this operation only reached about 50%, so this is not what we would call an ideal solution to the problem. When necessary, liquid metal residues were removed from the samples by dipping them in hydrochloric acid for a few seconds. The measurements on dielectric materials were done without liquid metal, in commercially made air lines.

The S-parameters of the air line with its material insert were measured for frequencies between 300 kHz and 20 GHz (0.2 GHz to 20 GHz for the dielectric materials), using two Hewlett-Packard network analysers, an HP 8753C and an HP 8720A. The frequency spectrum was divided into three ranges: 300 kHz to 20 MHz with a step size of 100 kHz, 20 MHz to 2 GHz with a 10 MHz step (both on the 8753C), and 200 MHz to 20 GHz with a 100 MHz step (on the 8720A; usually the values below 2 GHz were not used). For most measurements, the air line was connected to port 1 directly and to port 2 via a high-quality 7 mm cable in the case of the 8753C, or via high-quality test cables ending in 7 mm connectors for both ports in the case of the 8720A. Comparisons of the results with different cables and/or adapters suggested that it is not crucial to have a very low SWR in the parts of the measurement circuit that are calibrated out.

The network analysers were calibrated using the standard "full 2-port" calibration procedure with 7 mm calibration kits. The calibration procedure recommended by Hewlett-Packard was followed, with the exception that averaging was not always used during the isolation measurements. After connecting the air line, the reference planes were extended to the faces of the sample using the network analysers' port extension feature and the known lengths of the air line and sample. The sample was always placed at the port 1 end of the air line. In the 7 mm air lines, in which the centre conductor is spring-loaded, the sample location could not always be controlled very well; to ensure that the reference planes coincided with the faces of the sample, the phases of S_{11} and S_{22} were compared after extending the ports. In principle, S_{11} and S_{22} should be equal by symmetry; if the reference planes are offset from the sample faces, however, one would expect a phase difference between S_{11} and S_{22} that is proportional to the offset distance and the frequency. Observed phase differences were used to predict the offset and correct the port extensions. Typical corrections were of the order of 0.1 mm. Most of the measurements discussed herein were done with an averaging factor of 16.

The network analysers were interfaced to an HP 9816 computer via a GPIB bus. A BASIC program was written to control the S-parameter measurements and transfer the data to the computer. All four S-parameters were measured. After acquisition, the data were analysed on the computer using another BASIC program and/or transferred elsewhere for further analysis. More details on the BASIC programs (the first versions thereof, at least)

are given in a separate note [3].

4 Analysis Procedure

4.1 Resolving the Phase Ambiguity

After measuring the S-parameters over the desired frequency spectrum, we need to deduce ϵ and μ; they can be determined independently from the "forward" S-parameters (S_{11} and S_{21}) and the "reverse" S-parameters (S_{22} and S_{12}), since, by symmetry, we should have $S_{22} = S_{11}$ and $S_{12} = S_{21}$. It is straightforward to obtain μ and ϵ from equations (9) through (15), except for the $2\pi n/d$ uncertainty in the calculated value of k_z; we need to know the value of n at each frequency. Two methods are generally employed to resolve this dilemma; neither of these was used, for reasons that will be explained below. First, however, we will describe the method we actually did use.

It is convenient to divide the problem into two parts:

1. what is the correct value of n at the starting frequency in the spectrum?

2. at what frequencies must we change n as we sweep through the frequency spectrum?

The second part of the problem is the more straightforward. We can expect that if we choose a sufficiently small increment in frequency, $k_z d$ should be a smooth function of frequency. The principal value of $k_z d$, however (i.e. the value obtained assuming $n = 0$), will jump from a value near 2π to a value near 0 at frequencies where n increases by 1. This is illustrated in figure 2a for a typical case: the real part of $\mathcal{PV}(k_z d)/(2\pi)$ for ferrite-50 jumps from 1 to 0 at 12.5 GHz and 16 GHz. If we increment n at these frequencies, the jumps disappear completely (figure 2b). One would expect that n would only need to be incremented, but in some cases k_z actually decreases with increasing frequency, so decrementing n is sometimes necessary. Nevertheless, deciding when to increment or decrement n is straightforward under most circumstances, and can be done either by hand or using a simple automated algorithm.

The above approach may fail if the frequency steps are large enough for $k_z d$ to change by an appreciable fraction of 2π in one step; that was not a problem for the measurements discussed herein. The algorithm may also fail if the noise in the $k_z d$ data is an appreciable fraction of 2π, which was the case for some of the high-frequency measurements on the thicker samples of highly reflecting materials (evidently due to the fact that S_{21} was approaching the noise threshold of the analyser). Although alternate methods (such as the "Γ resonance" method mentioned below) might work better under these circumstances, data with this high noise level seemed not to be worth analysing.

The first part of the problem is a bit harder to pin down. If we are willing to admit that μ and ϵ may vary with frequency both inside and outside the frequency range of the measurement, then we cannot deduce the right starting value n_0 of n by measuring a single sample; since we have no way of knowing how many whole wavelengths fit in the sample length d at the starting frequency, any $n_0 \geq 0$ is possible (figure 3a). The only way to find

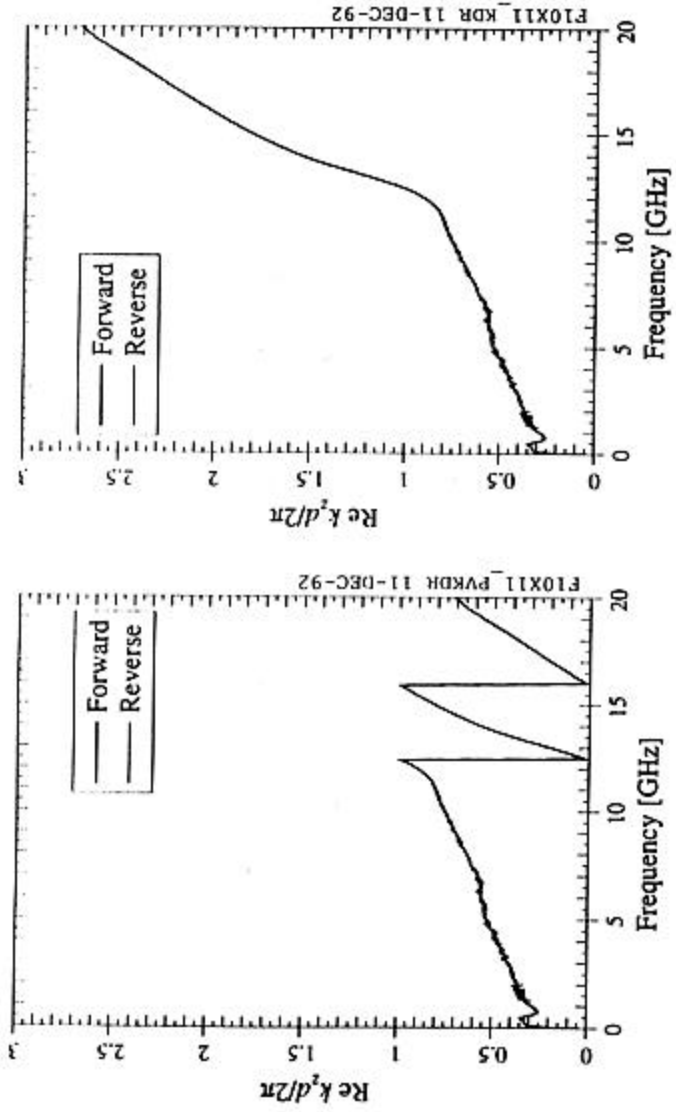

Figure 2. Measured values of the real part of $k_z d/(2\pi)$ for a ferrite-50 sample with $d = 9.8$ mm: (a) principal value of Re $k_z d/(2\pi)$; (b) Re $k_z d/(2\pi)$ with n incremented at 12.5 Ghz and 16 GHz, assuming an initial value $n_0 = 0$.

the right value of n_0 would seem to be through repeated measurements with different sample lengths: if we change d, we expect $k_z d$ to change but k_z to remain the same, provided we choose the correct n_0 value for each sample. As an example, results for the first few n_0 choices for three ferrite-50 samples of different length are shown in figure 3b. With $n_0 = 0$ for all three samples, the k_z values agree quite well. The choice of $n_0 = 1$ or 2 for the longest sample, on the other hand, is inconsistent with the other two samples. The choice of $n_0 = 3$ for the longest sample and $n_0 = 1$ for the intermediate sample are consistent with each other, but this choice is ruled out by the shortest sample, for which the first curve with $n_0 > 0$ has $k_z > 600$ m^{-1} (not shown in figure 3b). The choice of $n_0 = 0$ for all three samples seems the most sensible one, although we cannot exclude the possibility that larger values of n_0 may yield another consistent k_z curve (the first set of values that will even come close is $n_0 = 1$, 2, and 6, for the shortest, intermediate, and longest samples, respectively). We can never rule out completely the possibility of choosing the wrong n_0 values on the basis of different sample lengths; all we can do is increase our confidence in our choice of n_0 by measuring more samples of different lengths. The approach we followed was to assume $n_0 = 0$ (at the starting frequency of 300 kHz) for all of the materials, and then check the agreement between Re k_z values for different sample lengths. The agreement was reasonable in all cases.

Of course there is another way to find n_0—by already knowing k_z at one frequency. The properties of ferrite-50 have in fact been measured at 2.4 GHz using the resonator technique, which does not suffer from this sort of ambiguity, by our colleagues at Chalk River [8]. The result for Re k_z, also shown in figure 3b, does not agree exactly with the k_z values we obtain assuming $n_0 = 0$, but does definitely contradict the alternative choice of $k_z \geq 600$ m^{-1}.

As mentioned above, two other methods for finding n have been used. The first, introduced by Weir [2], is, in effect, to determine n by comparing the phase velocity to the group velocity[2]. His method can be understood quite easily in the context of the above discussion. From equation (2), we see that if $\mu\epsilon$ is independent of frequency, then Re k_z traces out a straight line passing through the origin. So for a material with constant μ and ϵ ("non-dispersive"), since we know the slope independently of n, (except at frequencies where n changes), we can easily determine the value of n that will make the line pass through $\omega = 0$ (see figure 28a in section 7 for an example). Obviously, this is an excellent way to deduce n, but since it only works for materials in which $\mu\epsilon$ is constant, it is not so useful for most of the materials measured herein, since their properties depend strongly on frequency.

The other method, used by Barry [7], is to make sure that the sample length is less than the wavelength

$$\lambda_z = \frac{2\pi}{\text{Re}\, k_z} \tag{17}$$

over the entire frequency spectrum. In practice, this is a reasonable solution because (as we will see in the next section) there are usually maxima in the measurement error near

[2] Weir actually expresses things in terms of delays rather than velocities, the group delay (which he calls "measured group delay" τ_g) and phase delay (which he calls "group delay at each frequency" τ_{pw}) being equal to the sample length divided by the group velocity and the phase velocity, respectively.

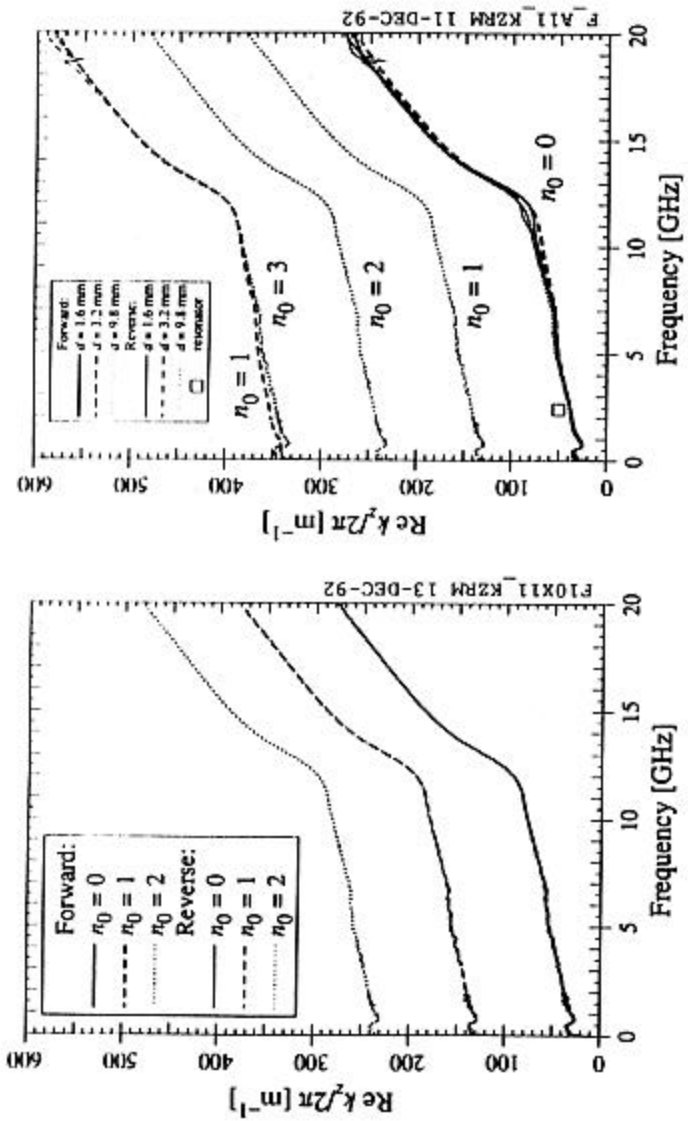

Figure 3. Measured values of the real part of the propagation wavenumber for ferrite-50, with n incremented as appropriate. (a) Re $k_z/(2\pi)$ for $d = 9.8$ mm, for some of the possible choices of n_0. (b) Re $k_z/(2\pi)$ for three different sample lengths, for some of the possible choices of n_0; a value measured using the resonator method [8] is also shown.

frequencies at which

$$d = \frac{m\lambda_z}{2}, \text{ for integer } m, \tag{18}$$

so samples shorter than λ_z usually produce better results. Nevertheless, because we were concerned about reproducibility between different samples and also needed to look at different sample lengths, we decided it was worthwhile to analyse data with $d \geq \lambda_z$.

Yet another alternative for choosing n is to examine the "resonances" one sees in Γ near frequencies at which equation (18) is satisfied. This method was tried in the first few measurements (see [3] for details), but was eventually abandoned because it does not work as well for absorbing materials and also because of the complication that one must be able to distinguish between resonances with even m, at which n changes, and odd m, at which n doesn't change.

4.2 Error Minimisation Strategies

There is one free parameter in the measurement, to wit the sample length d. We want to choose d so as to minimise the error in our μ and ϵ values. We followed the usual strategy for choosing d, a rationalisation for which can be found in [6]. We will repeat and expand upon this rationalisation in this section.

Consider first a material with purely real μ and ϵ, and hence purely real k_z (*i.e.* no attenuation). With k_z real, we have $|T| = 1$, and, according to equation (5), $T^2 = 1$ when d is an integer number of half wavelengths (equation (18)). From equations (7) and (8), we see that $S_{11} = 0$ and $S_{21} = \pm 1$ when $T^2 = 1$. Thus, we have full transmission and zero reflection when d satisfies equation (18). Under these circumstances, the directly reflected wave and the transmitted wave produced by the standing wave inside the material are equal in magnitude and out of phase by 180°, so they cancel completely, and all the power is transmitted. Because we get $S_{11} = 0$ and $S_{21} = \pm 1$ for any (real) μ and ϵ values when equation (18) is satisfied, we can expect to encounter difficulties when we try to calculate ϵ and μ. Indeed, we see from equation (11) that χ is 0/0 for these values of S_{11} and S_{21}. Thus, we can expect large fluctuations in values of χ and the corresponding values of Γ obtained via equation (9). The value of T, however, will not suffer large fluctuations, because it is independent of Γ when $S_{11} = 0$ and $S_{21} = \pm 1$, as the reader can easily check. Thus, we can expect large errors in Γ, and hence large errors in μ and ϵ, when d satisfies equation (18).

If the S-parameters are exactly correct, we should see these spikes in μ and ϵ only when equation (18) is satisfied exactly; since there will be always be some error in the measured S-parameters, however, we can expect enhanced errors in Γ when equation (18) is satisfied only approximately, so we will want to stay a safe distance away.

When μ and ϵ are not purely real, the attenuation in the wave as it travels through the sample will prevent us from satisfying $S_{11} = 0$ and $S_{21} = \pm 1$ exactly. However, S_{11} is still a minimum when d satisfies equation (18), and we have seen similar, albeit smaller, spikes in Γ at these frequencies in most of our measurements on absorbing materials.

We must also consider the error in T, or, equivalently, in k_z, when choosing d, a question about which we will be a bit more qualitative. Since Re $k_z d$ is the phase advance across the

sample, we would expect that, for a given error in the measured phases, we can reduce the error in Re k_z by increasing d. This is true as long as the attenuation through the sample does not become large enough to make it difficult to measure the transmitted phase. We can make a similar argument for Im k_z. Thus, we want to avoid having $d \ll \lambda_z$ or $d \gg 1/(\mathrm{Im}\, k_z)$. Because transmission can be measured more accurately than reflection, we can expect these bounds on d to be less important than the ones we obtained above.

In light of these considerations, we tried to satisfy the following condition as a rule of thumb in choosing the sample lengths:

$$\frac{\lambda_z}{8} \leq d \leq \frac{3\lambda_z}{8}. \tag{19}$$

The upper bound allows us to avoid getting near any frequencies at which $d = m\lambda_z/2$ for $m > 1$. The lower bound allows us to avoid having $d \ll \lambda_z$ or getting near $d = m\lambda_z/2$ for $m = 0$, although the choice of $\lambda_z/8$ was rather arbitrary (and difficult to adhere to strictly in many cases). Condition (19) allowed us to choose a single "best" sample length for each frequency in the spectrum.

The choice of d which minimises the error in Γ is not necessarily the same as the choice which minimises the error in k_z. This suggests that the best values of μ and ϵ could be obtained by measuring Γ and k_z with different sample lengths. We tried that approach with some materials; the results were not very different, probably due in part to the significant variations we see between different samples of the same material.

5 Results

Four varieties of nickel-zinc ferrite, three varieties of manganese-zinc ferrite, one non-ferrite absorbing material, and four dielectric materials were measured. Selected information on the materials is given in tables 1 and 2. There is significant variation in the properties of the TT2-111-series material, primarily due to the interest in higher DC conductivity that we expressed to the manufacturer. Additional information on the various varieties of the TT2-111-series material is given in table 3. Most measurements on TT2-111-series materials discussed herein were done on the TT2-111V variety. The variation in ferrite-50 properties was not as extreme, as can be seen in table 4.

5.1 Measurements on Dielectric Materials

To check the validity of our techniques, teflon, air, K-7, and K-10 were measured between 0.2 and 20 GHz. Teflon has been measured previously by several researchers using the transmission line technique [2, 6, 7]. The properties of these dielectrics are different enough from the absorbing materials that being able to measure their μ and ϵ correctly is not sufficient to ensure that we can measure the absorbing materials' properties correctly, but it is still a worthwhile exercise.

Results for three teflon samples are shown in figures 4 and 5. Both forward (calculated from S_{11} and S_{21}) and reverse (calculated from S_{22} and S_{12}) values of μ and ϵ are shown.

Table 1. Manufacturer, material type, and stated resistivity of the absorbing materials under study.

Material	Manufacturer	Type	DC Resistivity [Ωm]
Ferrite-50	Trans-Tech	Nickel-zinc	$0.25\ ^{+0.75}_{-0.15}$
TT2-111-series[a]	Trans-Tech	Nickel-zinc	8 to 10^3
CMD10	Ceramic Magnetics	Nickel-zinc	10^3
IB-004	TDK[b]	Nickel-zinc[c]	
MN60	Ceramic Magnetics	Manganese-zinc	2
MN67	Ceramic Magnetics	Manganese-zinc	1.5
MN80	Ceramic Magnetics	Manganese-zinc	2
Al-N-C	Ceradyne[d]	Non-ferrite[e]	

[a] resistivity varies, see table 3
[b] material was sent by T. Tajima (KEK)
[c] The composition of IB-004 is undisclosed, but we have classified it as nickel-zinc herein for simplicity
[d] material was sent by I. E. Campisi (CEBAF)
[e] glassy carbon in aluminum nitride

Table 2. Manufacturer and properties of the dielectric materials under study. Air ($\epsilon/\epsilon_0 \simeq 1$, $\mu/\mu_0 \simeq 1$) was measured also. K-7 and K-10 are used to model the microwave properties of beryllium oxide and alumina.

Material	Manufacturer	Microwave Properties
Teflon (virgin grade)	Dupont	$\epsilon/\epsilon_0 \simeq 2$, $\mu/\mu_0 \simeq 1$
K-7 stycast	Emerson & Cuming	$\epsilon/\epsilon_0 \simeq 7$, $\mu/\mu_0 \simeq 1$
K-10 stycast	Emerson & Cuming	$\epsilon/\epsilon_0 \simeq 10$, $\mu/\mu_0 \simeq 1$

Table 3. Stated resistivity of various varieties of TT2-111-series materials received from Trans-Tech. Trans-Tech's designation for all varieties is TT2-111R.

Lot Number	DC Resistivity [Ωm]	LNS Designation
70 347	10^3	TT2-111R
74 837	449	TT2-111C-I
74 898	842	TT2-111C-II
75 074	59.0	TT2-111U
75 575	435	TT2-111V
75 576	125	TT2-111S
78 263	7.84	

Table 4. Stated resistivity of various lots of ferrite-50 received from Trans-Tech.

Lot Number	DC Resistivity [Ωm]
68 497	0.397
70 838	0.173
73 595	0.142
73 627	0.347
77 871	0.501

Large spikes can been seen in the values near 4.4, 8.6, 12.8, and 17 GHz for the longest sample and at about 13.5 GHz for the intermediate sample. As expected, these spikes occur when d satisfies equation (18). There is also a smaller spike near 15.2 GHz in the results for the longest sample that is apparently unrelated to equation (18). Aside from the spikes, the results agree on average with the expected values, though the deviations are still significant.

Results for the other three dielectric materials are shown in figures 6 and 7. The sample length for the air measurement was 50 mm (the length of the air line); the K-7 and K-10 samples both had $d = 6.6$ mm. The results are similar to the teflon results: they agree with the expected value on average, with large spikes when d is an integer number of half wavelengths.

The results for air agree the best with the expected values, probably due to the fact that there are no problems associated with the machining of the sample. We found that the results for the other dielectric materials did depend strongly on how well the samples fit into the air line. We did not try to improve the machining of the dielectric samples very much, as the machining problems for these materials are quite different from the problems encountered with the absorbing materials. We did not try using liquid metal with the dielectric materials either. Our results for the dielectrics suggest that our measurement techniques are valid, but sensitive to the fit between the sample and air line, and susceptible to large errors for some combinations of sample length and wavelength.

5.2 Sample-by-Sample Measurements of Absorbing Materials

The μ and ϵ values were measured for two or more samples of different length for each microwave-absorbing material. For all measurements discussed in this section, different samples of the same material were machined from the same piece of material (with the possible exception of ferrite-50). Forward (from S_{11} and S_{21}) and reverse (from S_{22} and S_{12}) values of μ and ϵ for each sample are shown for two nickel-zinc materials in figures 8 through 11. The detailed results for the other materials are given in the appendix.

For nickel-zinc ferrites, the values of μ agree quite well with each other under most circumstances. Noticeable disagreement between different samples (and between forward and reverse values) can be seen at very low frequencies and when the real or imaginary part of μ is close to zero. At low frequencies, the values for the longest sample usually show the lowest amount of noise, which supports the contention that we need to avoid $d \ll \lambda_z$ or $d \ll 1/(\mathrm{Im}\, k_z)$; for most of the nickel-zinc ferrites (with the exception of ferrite-50), we approach full transmission of the incident wave ($S_{11} = 0$ and $S_{21} = 1$) at low frequencies, so that we are deducing μ and ϵ by taking the subtracting numbers that are almost equal. Fortunately for us, the rapid increase in μ and ϵ as the frequency decreases prevents λ_z from increasing as fast as it would ordinarily, thereby giving us better results at low frequencies than we might expect for our relatively short sample lengths. Disagreements for small $\mathrm{Re}\,\mu$ or $\mathrm{Im}\,\mu$ are to be expected if we assume the magnitude and phase of μ both have some error associated with them. At the high-frequency end of the spectrum, there are spikes in the calculated values of μ for most of the longer samples at frequencies where d is an integer multiple of λ_z, where the aforementioned resonances in the measured values of Γ occur.

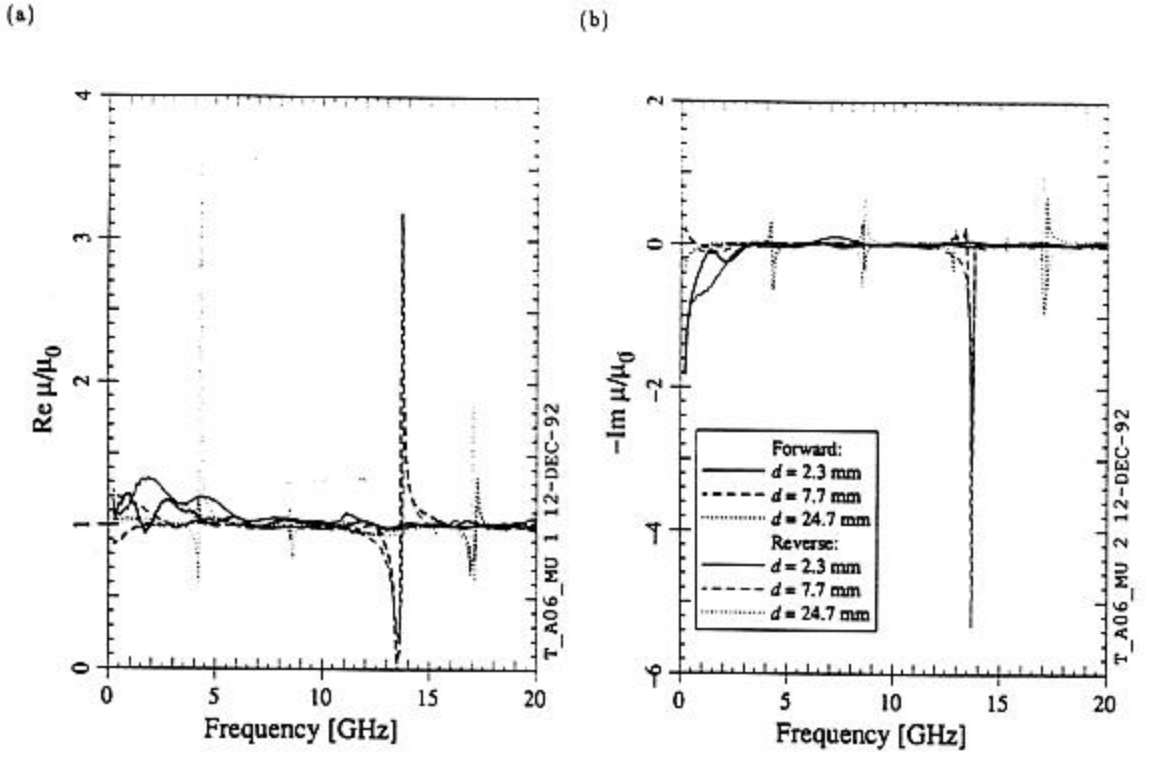

Figure 4. Measured values of (a) the real part and (b) the imaginary part (times -1) of μ for three teflon samples.

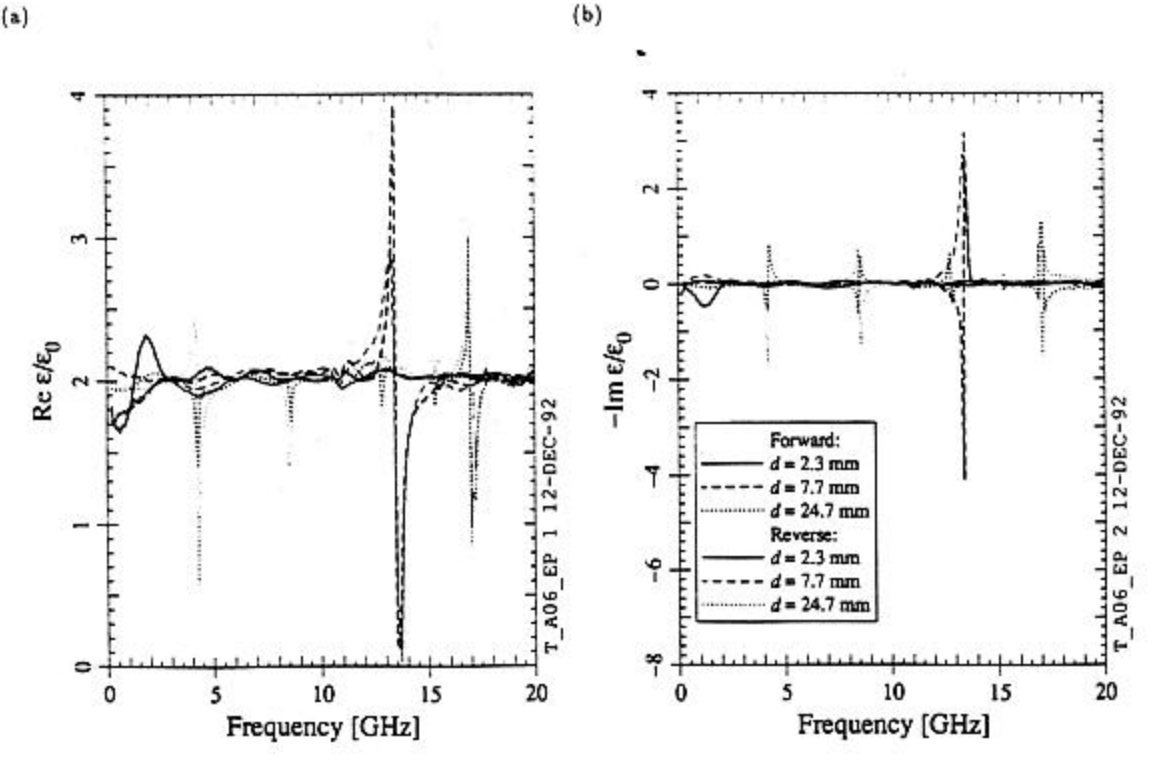

Figure 5. Measured values of (a) the real part and (b) the imaginary part (times -1) of ϵ for three teflon samples.

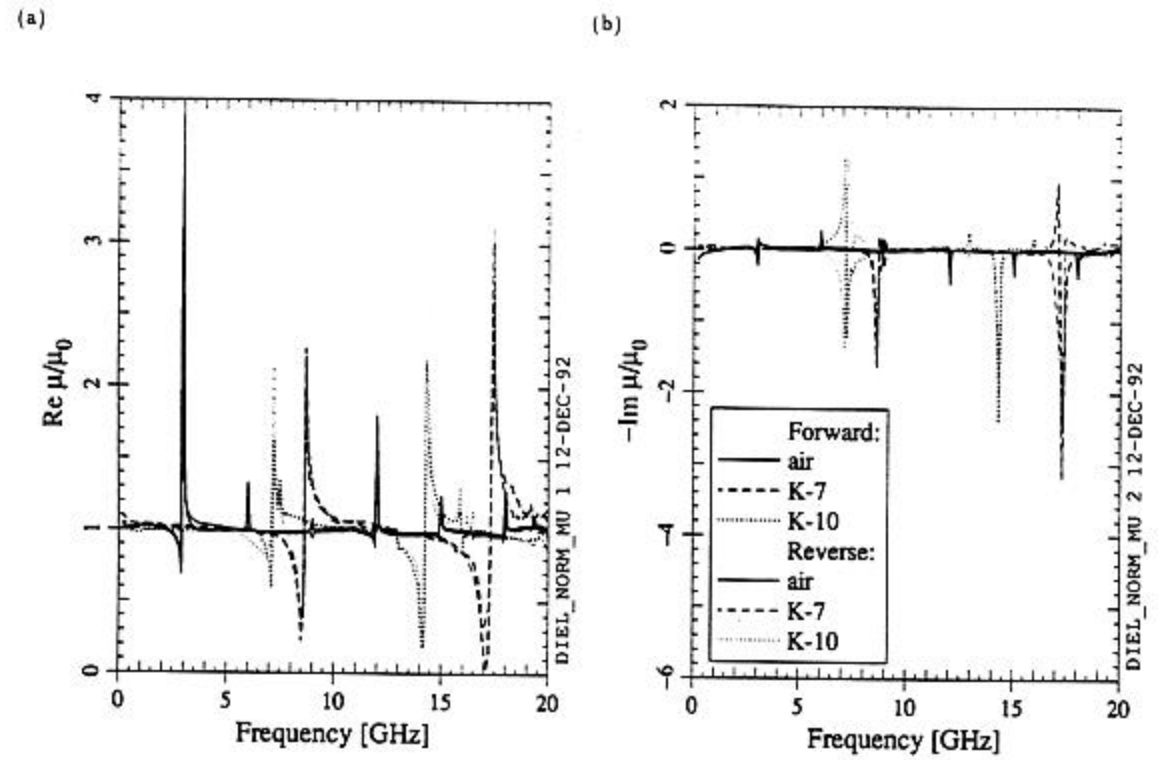

Figure 6. Measured values of (a) the real part and (b) the imaginary part (times -1) of μ for samples of three dielectric materials.

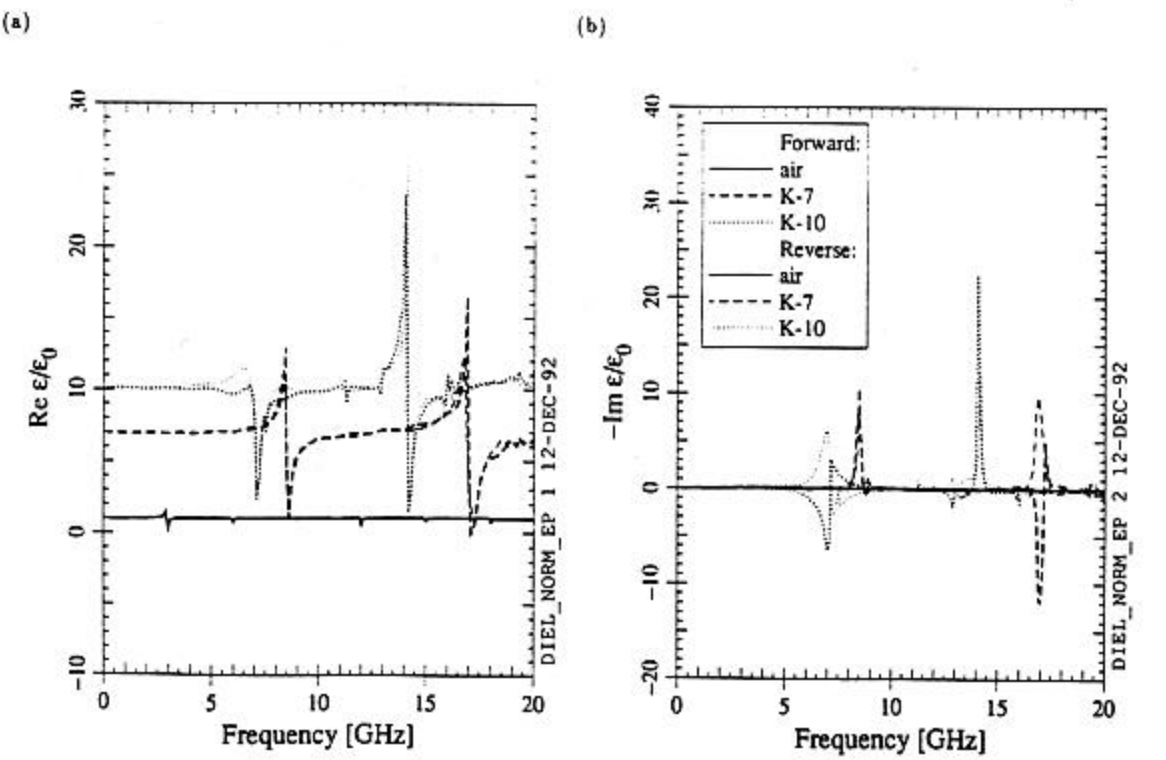

Figure 7. Measured values of (a) the real part and (b) the imaginary part (times -1) of ϵ for samples of three dielectric materials.

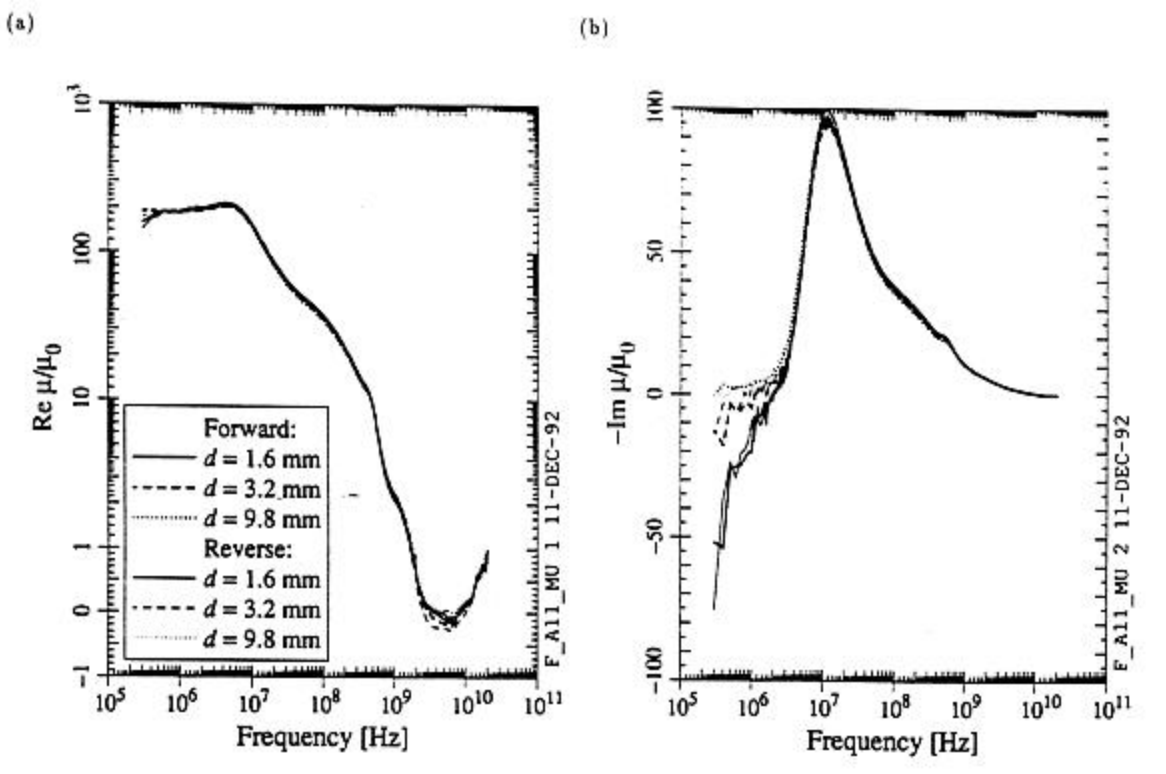

Figure 8. Measured values of (a) the real part and (b) the imaginary part (times −1) of μ for three ferrite-50 samples.

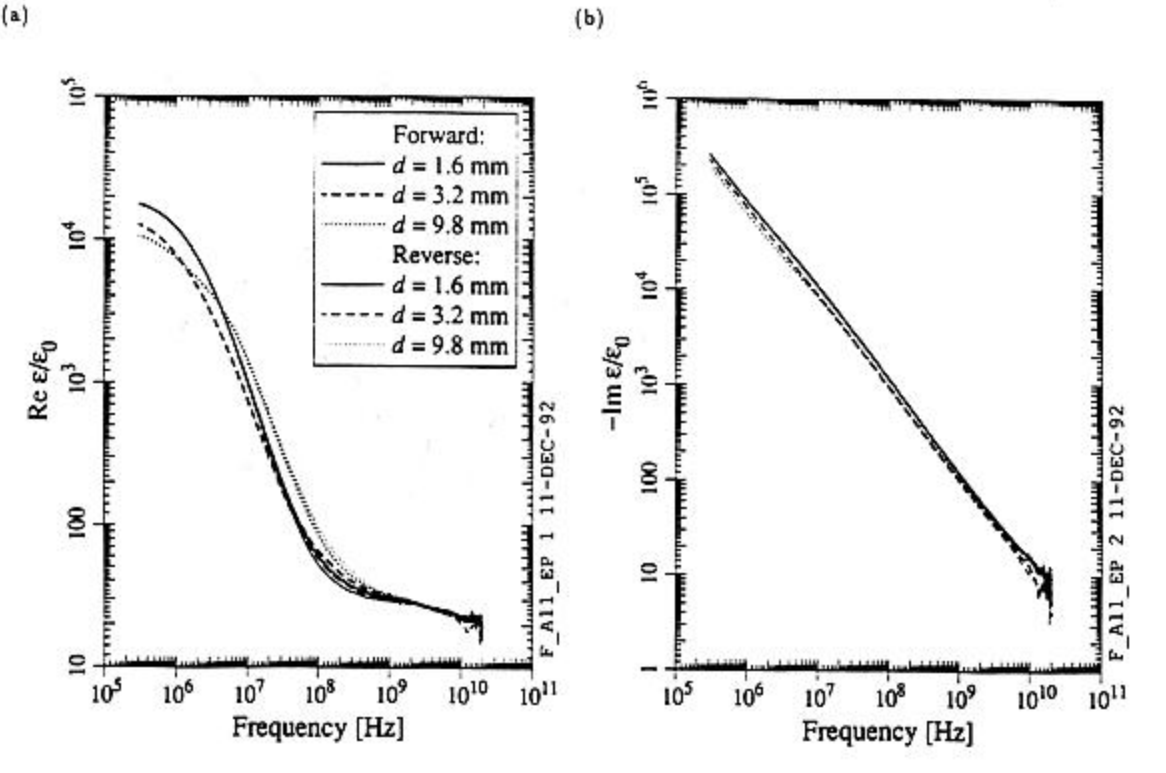

Figure 9. Measured values of (a) the real part and (b) the imaginary part (times −1) of ϵ for three ferrite-50 samples.

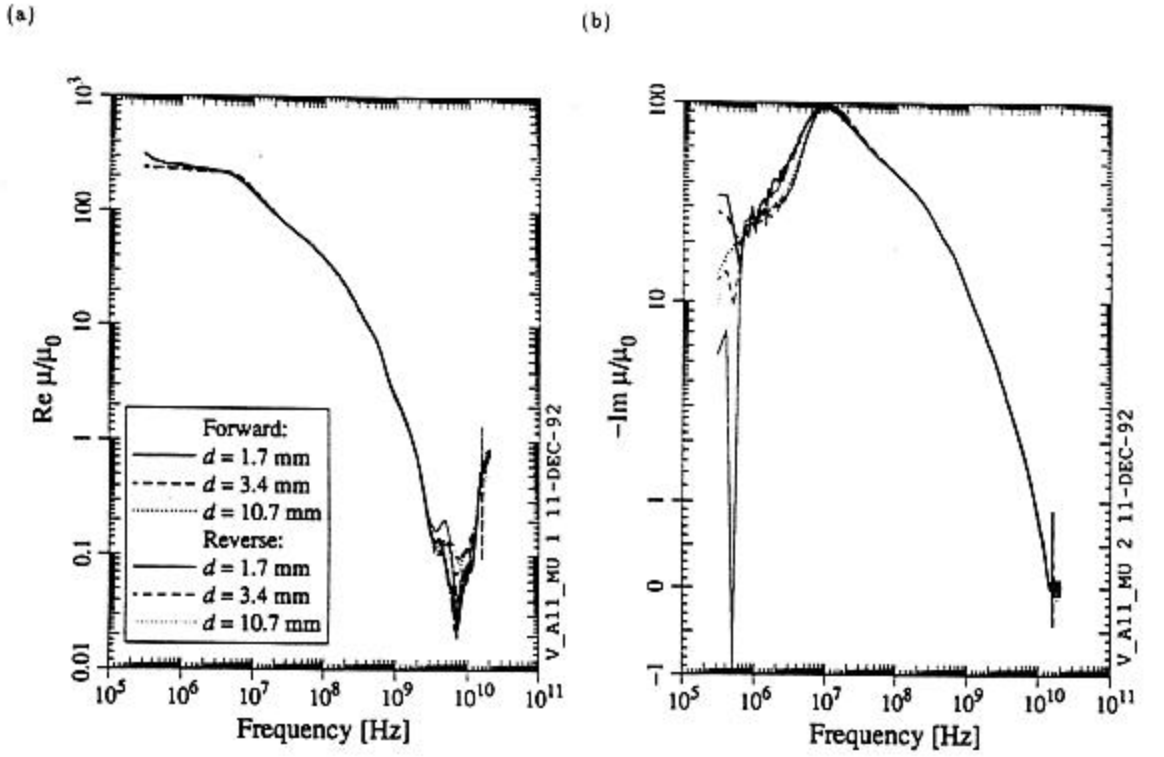

Figure 10. Measured values of (a) the real part and (b) the imaginary part (times −1) of μ for three TT2-111V samples.

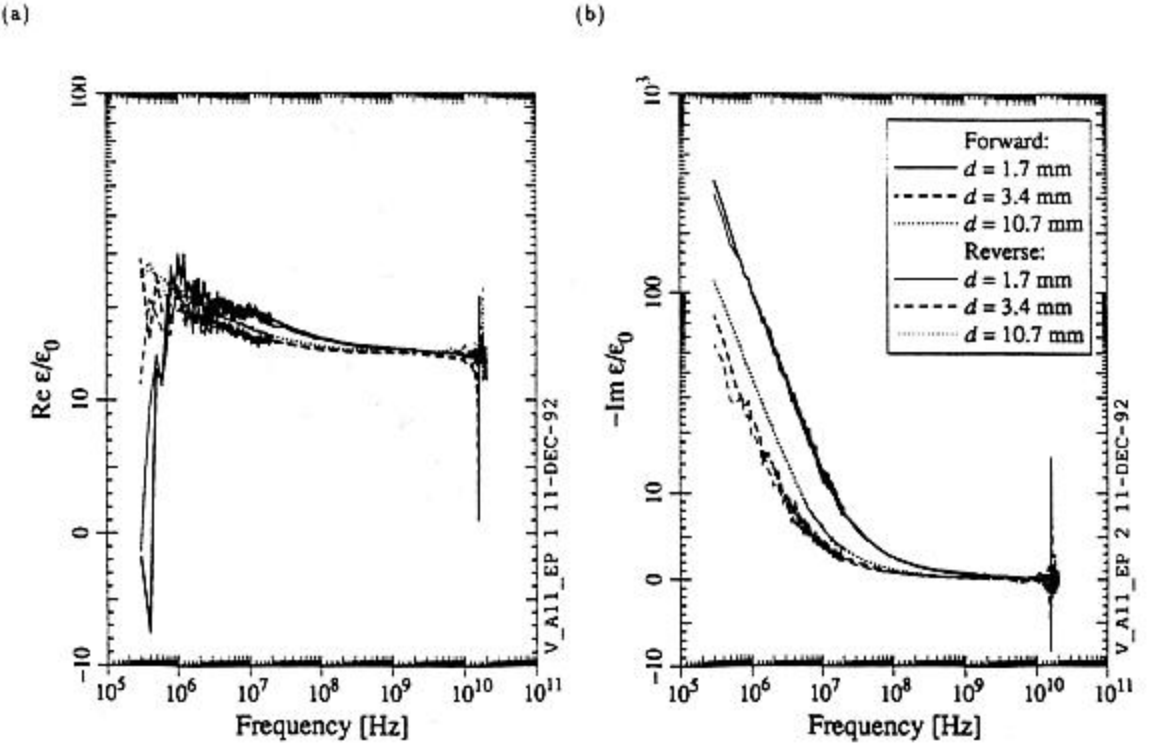

Figure 11. Measured values of (a) the real part and (b) the imaginary part (times −1) of ϵ for three TT2-111V samples.

The above observations apply equally well to the ϵ results for the nickel-zinc ferrites. Systematic differences in the calculated ϵ values for different samples can also be seen, particularly when Re ϵ or Im ϵ is large. The most extreme case is TT2-111V, for which Im ϵ values differ by about a factor of five at low frequencies.

Measuring the manganese-zinc ferrites proved to be more challenging. The magnitude of Γ was close to 1 over a large frequency range for these materials, so that only a small fraction of the incident wave was transmitted, making the error in the calculated values of k_z large. Reducing the sample length and taking an average of several S-parameter traces helped improve the results, but did not eliminate noise problems completely. With Don Metzger's guidance, we learned that the averaging did not improve the measurement unless averaging was also used during the isolation calibration of the analyser. The remaining noise in the results is still correlated with low transmission through the sample (i.e. $|S_{21}| \ll 1$). For some of the longer samples, the noise in Re k_z became large enough at higher frequencies to make it difficult to determine when to increment n, which is why some of the curves shown in the appendix do not extend all the way to 20 GHz. The agreement between the results for different sample lengths is rather poor in some cases, especially for MN60 and MN67. It would be worthwhile to do some more measurements to see whether better reproducibility can be found. Measurements on even shorter samples would be desirable, because our shortest samples do not yet satisfy $d < \lambda_z/2$ at the high-frequency end of the spectrum. Machining and measuring samples shorter than 0.8 mm may be difficult, however.

The results for the Al-N-C material show phenomena similar to the results for the nickel-zinc ferrites: disagreement and noise in the values at low frequencies, systematic differences in ϵ values, and spikes at high frequencies.

5.3 Composite Results for Absorbing Materials

We used condition (19) to help choose the best sample length for each frequency, dividing the frequency spectrum into several ranges. The forward and reverse values were still treated as independent in order to get some indication of the accuracy.

Our "best guess" values of μ and ϵ for ferrite-50 are shown in figures 12 and 13. The worst agreement between forward and reverse is seen when values are close to zero, especially at low frequencies. The observant reader will notice some small steps in the values (particularly visible in Im ϵ). These occur at the frequencies at which we change our choice of sample, and are due to the systematic differences between results for different samples seen in the previous section. Such steps will be seen in the results for most of the materials. Values measured for ferrite-50 at 2.4 GHz using the resonator method [8] are also shown in figures 12 and 13. The resonator results agree relatively well with ours.

Best guesses for the other nickel-zinc ferrites are shown in figures 14 and 15. Similar observations can be made about the results. The most noisy values are again at low frequencies, especially for the CMD10 and IB-004 materials, for which material was not available to make samples as long as would have been desirable. Both the real and imaginary parts of ϵ are quite a bit smaller in these materials compared with ferrite-50. In CMD10 and IB-004, Im ϵ is small enough to make it difficult to measure with this technique. The real

and imaginary parts of μ follow the same trends in all four nickel-zinc materials, albeit with some differences.

Best guesses for the manganese-zinc ferrites are shown in figures 16 and 17. There is a significant amount of noise in the measured values at higher frequencies, particularly in the real parts of μ and ϵ. The reproducibility problems between different MN67 samples also produce some large jumps in the values. It is clear, nevertheless, that all components are much larger than for the nickel-zinc ferrites, the only exception being the Im ϵ values, which are of the same order as for ferrite-50.

Best guesses for the Al-N-C material are shown in figures 18 and 19. Low-frequency errors are especially pronounced in the results because μ and ϵ are much smaller (compared to the ferrite materials) at low frequencies; good low-frequency measurements for this material would necessitate sample lengths that are much longer than what we have succeeded in producing so far. If we discount the low-frequency effects, it is difficult to say much about μ except that $\mu \sim \mu_0$ to the accuracy of the measurement.

6 Discussion

6.1 General Comments

The signs of the real and imaginary parts of μ and ϵ agree with our expectations for the most part: the real parts is are positive (so that the electromagnetic energy stored in the materials is positive) most of the time; and the imaginary parts are negative (so that the materials absorb electromagnetic energy) most of the time.

Ferrite-50 differs from the other nickel-zinc ferrites mostly in its ϵ values. All of the manganese-zinc ferrites have μ and ϵ values that are much larger in magnitude than the nickel-zinc ferrites. All of the ferrites share the trend of values that decrease with increasing frequency, with only a few exceptions.

The measured values of μ and ϵ in the ferrites show features that might be considered extreme: significant variation with frequency, large values at low frequencies (as large as 10^6), and very small values at high frequencies under some circumstances, with Re μ sometimes less than 1 (or even 0). These phenomena may shock some readers; nevertheless, all of these features have been seen in previous measurements of nickel-zinc ferrites [9]. The result that Re $\mu < 1$ may be correct; it is confirmed by the resonator measurement on ferrite-50 at 2.4 GHz (see figure 12). The results that Re $\mu < 0$ in some circumstances may be due to systematic error.

The observant reader may have noticed that the measured real part of the propagation wavenumber for ferrite-50 decreases with increasing frequency over a narrow range of frequencies near 500 MHz (see figure 3), meaning that the group velocity is negative in that frequency range. Several other ferrites, the manganese-zinc ones in particular, also show a negative group velocity over a limited frequency range. The imaginary part of k_z is always relatively large near frequencies where the group velocity is negative, which means that travelling waves are strongly attenuated. We believe that this negative group velocity is a real

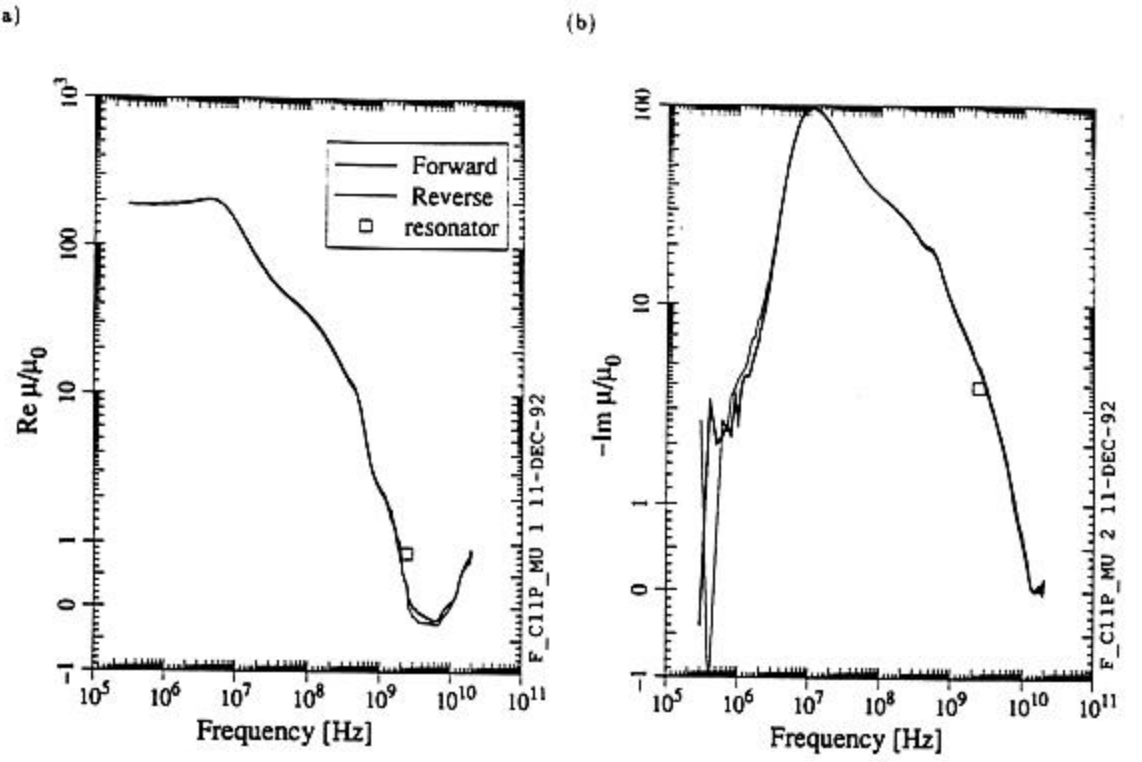

Figure 12. Composite of measured values of (a) the real part and (b) the imaginary part (times -1) of μ for ferrite-50. Values measured using the resonator method [8] are also shown.

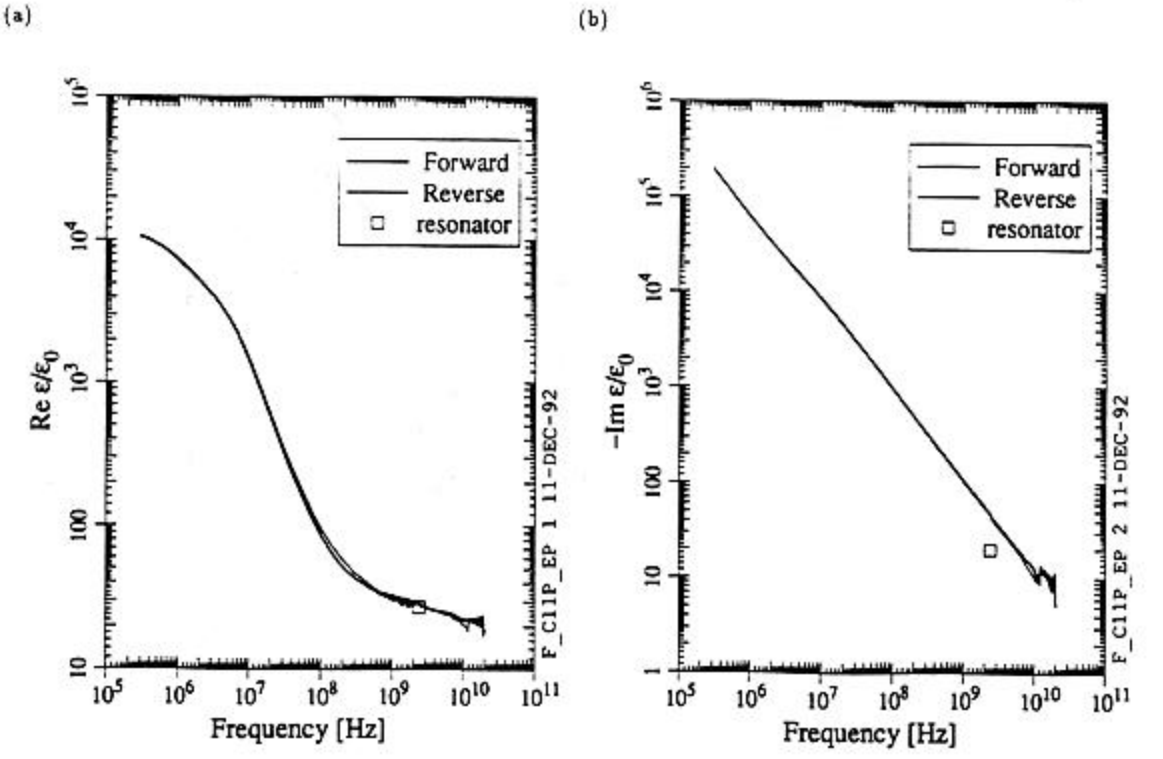

Figure 13. Composite of measured values of (a) the real part and (b) the imaginary part (times -1) of ϵ for ferrite-50. Values measured using the resonator method [8] are also shown.

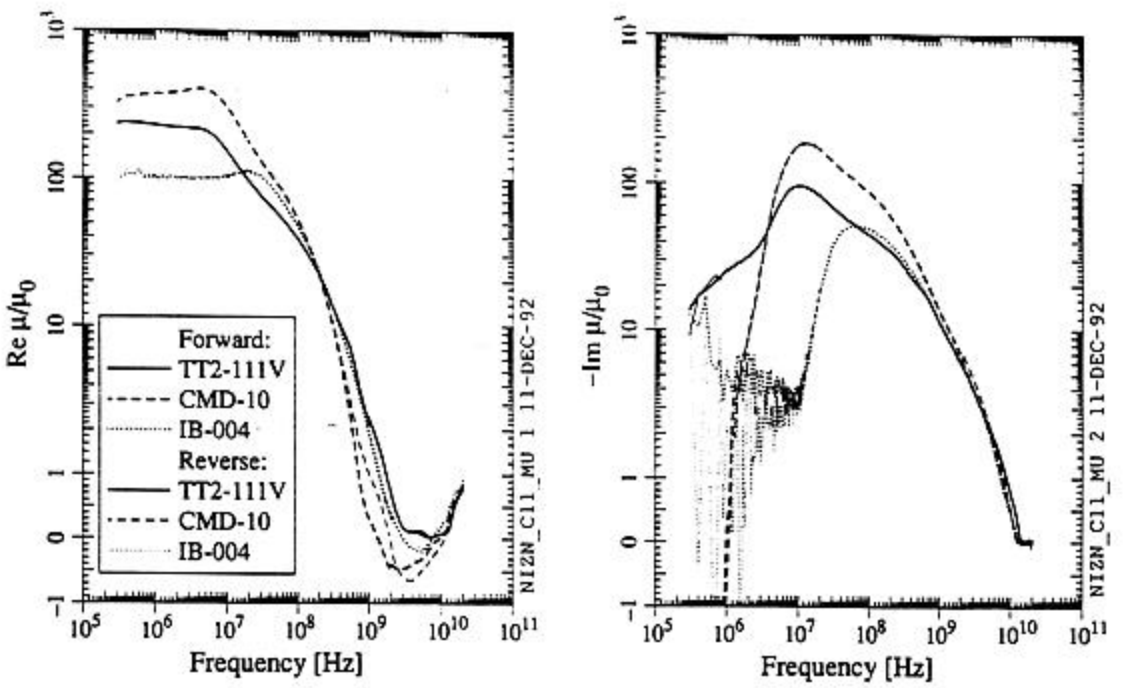

Figure 14. Composite of measured values of (a) the real part and (b) the imaginary part (times −1) of μ for TT2-111V, CMD10, and IB-004 ferrites.

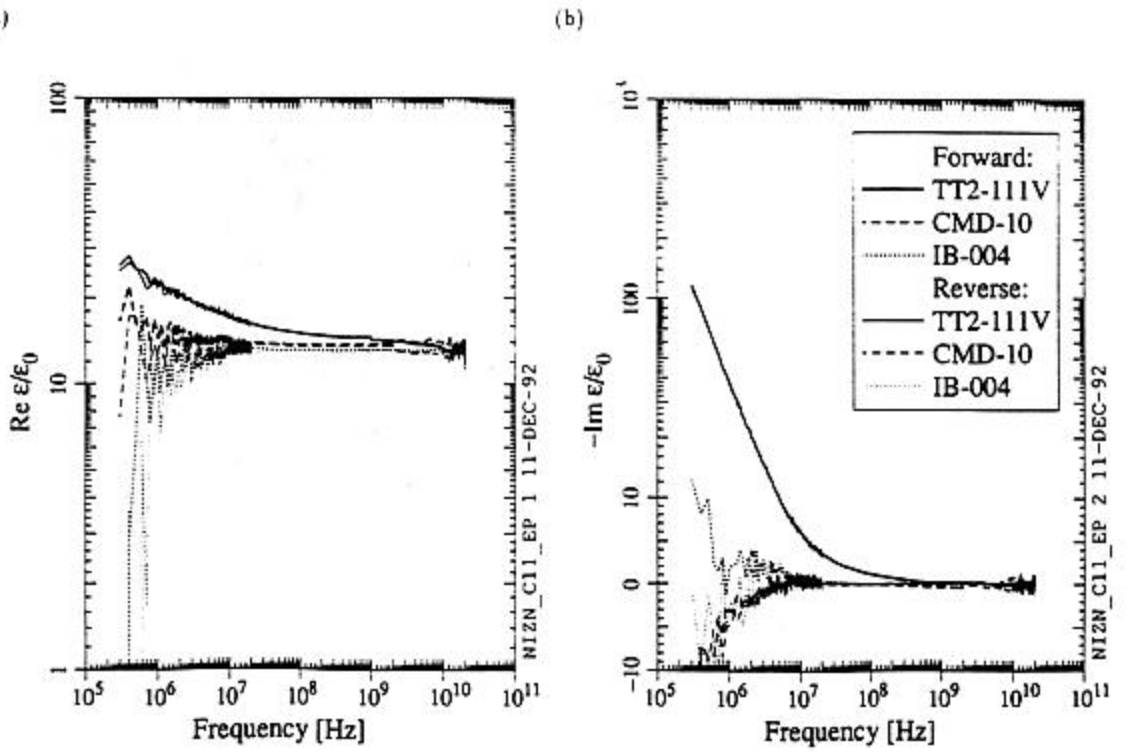

Figure 15. Composite of measured values of (a) the real part and (b) the imaginary part (times −1) of ϵ for TT2-111V, CMD10, and IB-004 ferrites.

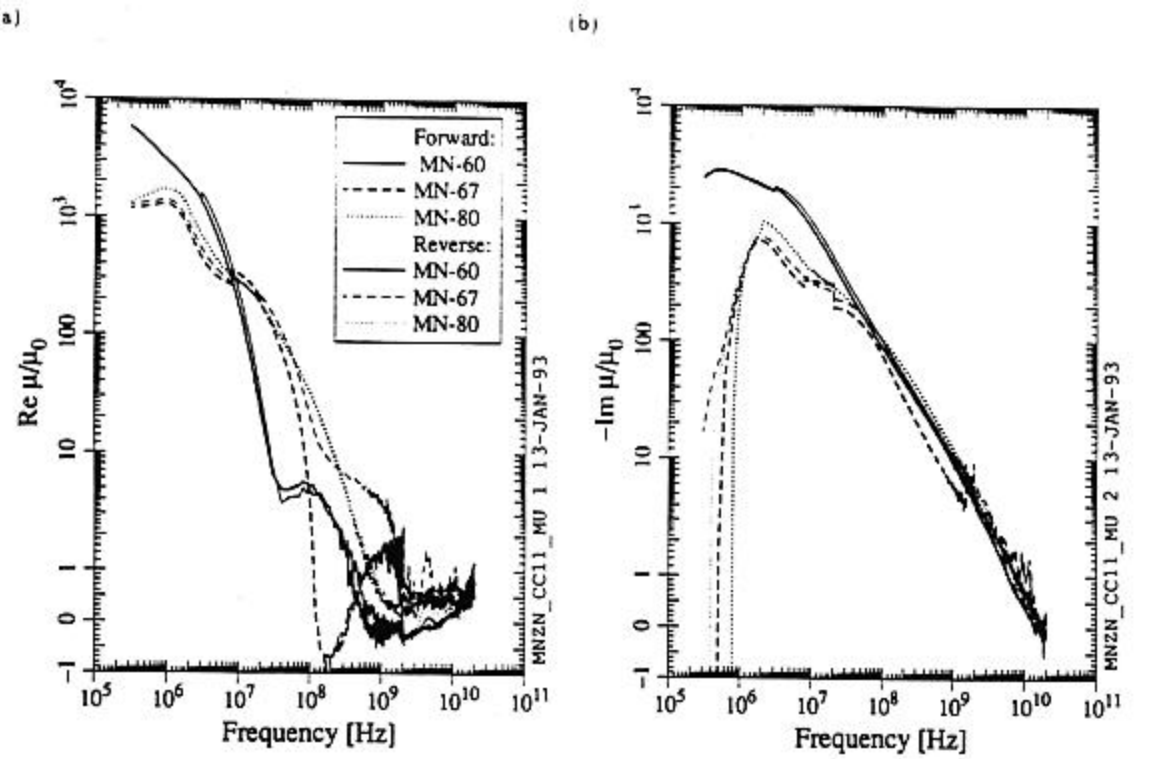

Figure 16. Composite of measured values of (a) the real part and (b) the imaginary part (times −1) of μ for MN60, MN67, and MN80 ferrites.

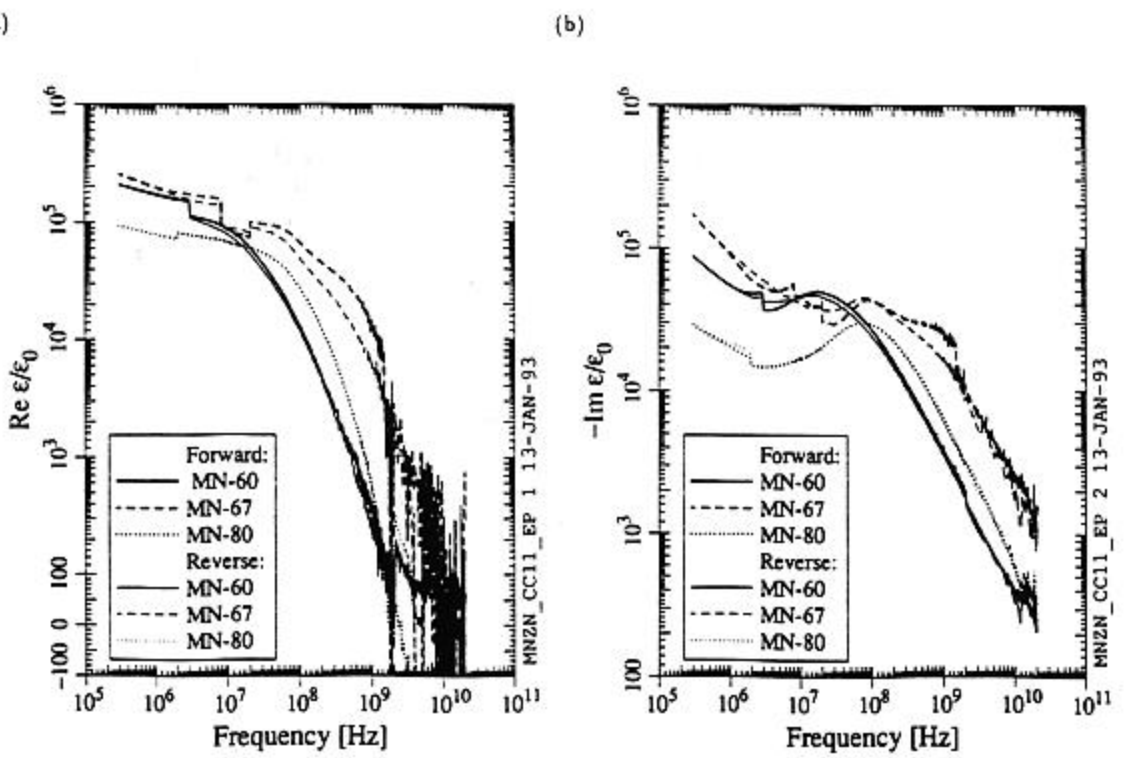

Figure 17. Composite of measured values of (a) the real part and (b) the imaginary part (times −1) of ϵ for MN60, MN67, and MN80 ferrites.

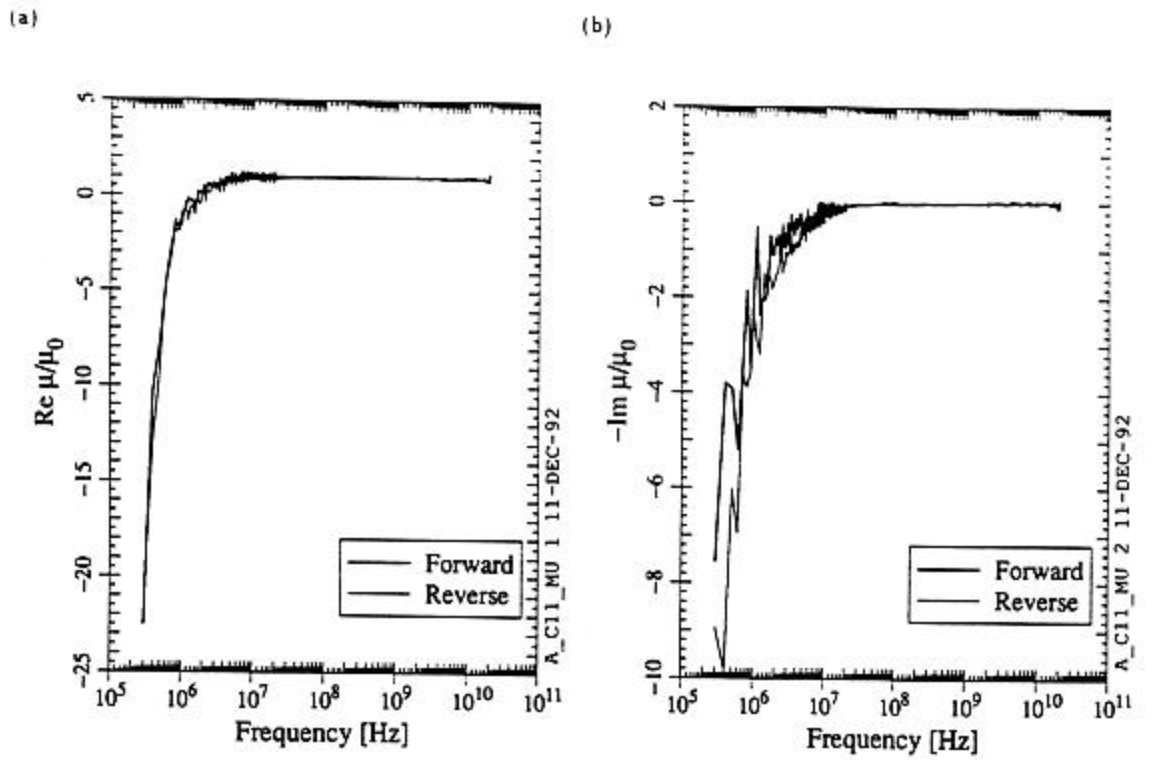

Figure 18. Composite of measured values of (a) the real part and (b) the imaginary part (times −1) of μ for the Al-N-C material.

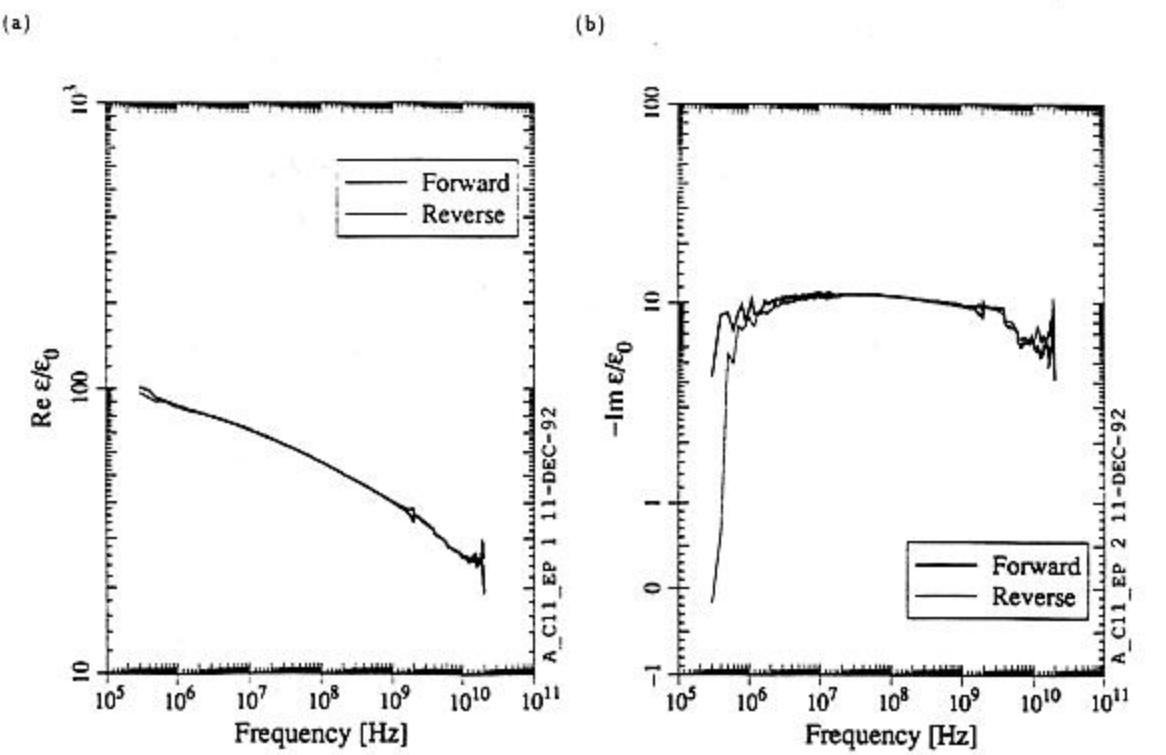

Figure 19. Composite of measured values of (a) the real part and (b) the imaginary part (times −1) of ϵ for the Al-N-C material.

effect. It is known to occur in some ferrites (biased ones, at least) [10].

Barry [7] has measured the properties of NZ-51 material from Emerson & Cuming, which, we have been informed [11], is similar to Trans-Tech's TT2-111-series material. He used the transmission line technique with *TEM* waves in a stripline, measuring μ and ϵ between 500 MHz and 5.5 GHz. Our results for TT2-111V are quite close to his, though not exactly the same; our measured values of Re ϵ, for example, are a bit larger.

6.2 Air Gaps and their Influence on the Measurement

The presence of air gaps between the sample and air line was found to have a strong effect on the measured values of ϵ, particularly for materials which have a large ϵ, such as ferrite-50. Systematic measurements were done for three cases: (i) samples machined without tight tolerances, which fit loosely inside the air line (rounds 2, 3, and 4), (ii) samples with tighter tolerances, which fit snugly inside the line (round 6), and (iii) samples with slightly relaxed tolerances, but with liquid metal present in the gap between the sample and air line (round 11). The results for samples of ferrite-50 and TT2-111-series ferrite of length ~ 1.6 mm are compared in figures 20, 21, 22 and 23. For both materials, the agreement between μ values measured in different rounds is more or less reasonable. On the other hand, the ϵ values for ferrite-50 change dramatically between rounds; this is true to a lesser extent for the TT2-111-series ferrite. The effect is most pronounced for the largest ϵ values. In principle, the measurements with the smallest air gaps are the most trustworthy, since we assume in the analysis that the material fills the air line completely. In addition, the reproducibility of the results for different samples was found to improve in going from method (i) to method (iii); as mentioned previously, however, the reproducibility of the measurement is not outstanding, even with the liquid metal filling the gaps.

With guidance from Vadim Veshcherevich and Linda Walling, we can provide a qualitative explanation of the air gap effect with a simple static analysis of a partially filled transmission line. The analysis will be valid in the long wavelength limit. In this limit, the propagation wavenumber and characteristic impedance of a transmission line are determined by the inductance per unit length L' and the capacitance per unit length C':

$$k_z = \pm\omega\sqrt{L'C'} \tag{20}$$

$$Z = \pm\sqrt{\frac{L'}{C'}}. \tag{21}$$

Thus, in this limit, L' and C' are the quantities that can be directly determined by measuring k_z and Z. In the case of a coaxial line that is completely filled with a material of permeability μ and permittivity ϵ, it is easy to show that

$$L' = \frac{\ln\left(\frac{b}{a}\right)}{2\pi}\mu \tag{22}$$

$$C' = \frac{2\pi}{\ln\left(\frac{b}{a}\right)}\epsilon, \tag{23}$$

where a and b are the radii of the inner and outer conductors, respectively. So, for a filled line, it is easy to deduce μ and ϵ from L' and C'. Equations (20) through (23) reduce to the expressions given earlier for k_z and Z (note that $Z_0 = \sqrt{\mu_0/\epsilon_0}\ln(b/a)/(2\pi)$ in the coaxial case).

Let us now consider a line that is only partially filled with material; suppose there are air gaps between the inner and outer conductors and the material. In that case, equations (22) and (23) no longer apply. In the static limit, we can derive exact expressions for inductance and capacitance in such a configuration, as long as the geometry remains axisymmetric. Assuming that the air gaps are small compared to a and b, we get relatively simple expressions for L' and C':

$$L' = \frac{1}{2\pi}\left[\mu\ln\left(\frac{b}{a}\right) + \mu_0\left(\frac{\delta_i}{a} + \frac{\delta_o}{b}\right)\right] \tag{24}$$

$$C' = 2\pi\left[\frac{1}{\epsilon}\ln\left(\frac{b}{a}\right) + \frac{1}{\epsilon_0}\left(\frac{\delta_i}{a} + \frac{\delta_o}{b}\right)\right]^{-1}, \tag{25}$$

where δ_i and δ_o are the lengths of the gaps from the material to the inner and outer conductors, respectively. Equations (24) and (25) demonstrate that the simple expressions for ϵ and μ that we use in the analysis are not strictly valid if air gaps are present. The correction terms vanish as δ_i and δ_o go to zero, as they should.

Let us examine first the relationship between L' and μ. Since $\ln(b/a)$ is typically of order 1, the correction term in equation (24) will always be small as long as the gaps are small compared to a and b and as long as μ is not small compared to μ_0. Thus we can expect that air gaps will not have a strong influence on measured μ values under most circumstances (we sometimes measure μ values smaller than μ_0; this analysis casts some doubt on their accuracy). For C' and ϵ, things are different: assuming again that $\ln(b/a)$ is of order 1, the correction term in equation (25) will be small if the gaps are small compared to a and b and ϵ is not *large* compared to ϵ_0. If ϵ/ϵ_0 is an appreciable fraction of a/δ_i or b/δ_o, we can expect a significant correction due to the air gaps. Both conclusions agree well with our earlier observation that air gaps have little influence on measured values of μ and significant influence on measured ϵ values for large ϵ.

6.3 Reproducibility

To help identify the source of the nonreproducibility between measurements on samples of different lengths, three measurements on TT2-111V were compared: (i) a first measurement on a short sample, (ii) a second measurement on the same sample, done after removing and re-applying the liquid metal, and (iii) a measurement on a different sample of about the same length. The results are shown in figures 24 and 25. The μ results for the three cases do not show much systematic difference. On the other hand, the two measurements of ϵ for the same sample agree significantly better with each other than they do with the measurement on the other sample. Similar agreement between repeated measurements on a longer sample was also seen. This indicates that the lack of reproducibility stems primarily

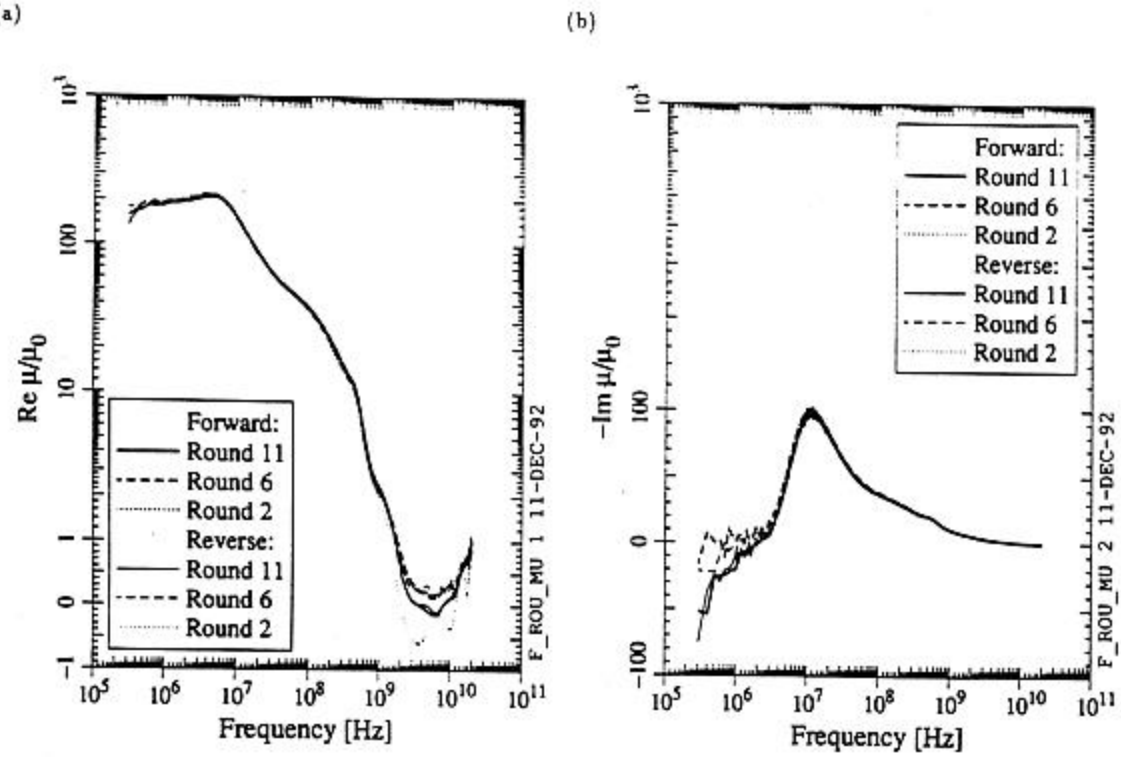

Figure 20. Comparison of the results of different rounds of measurements of (a) the real part and (b) the imaginary part (times -1) of μ for ferrite-50. The fit between the sample and air line was improved in round 6 and liquid metal was used in round 11.

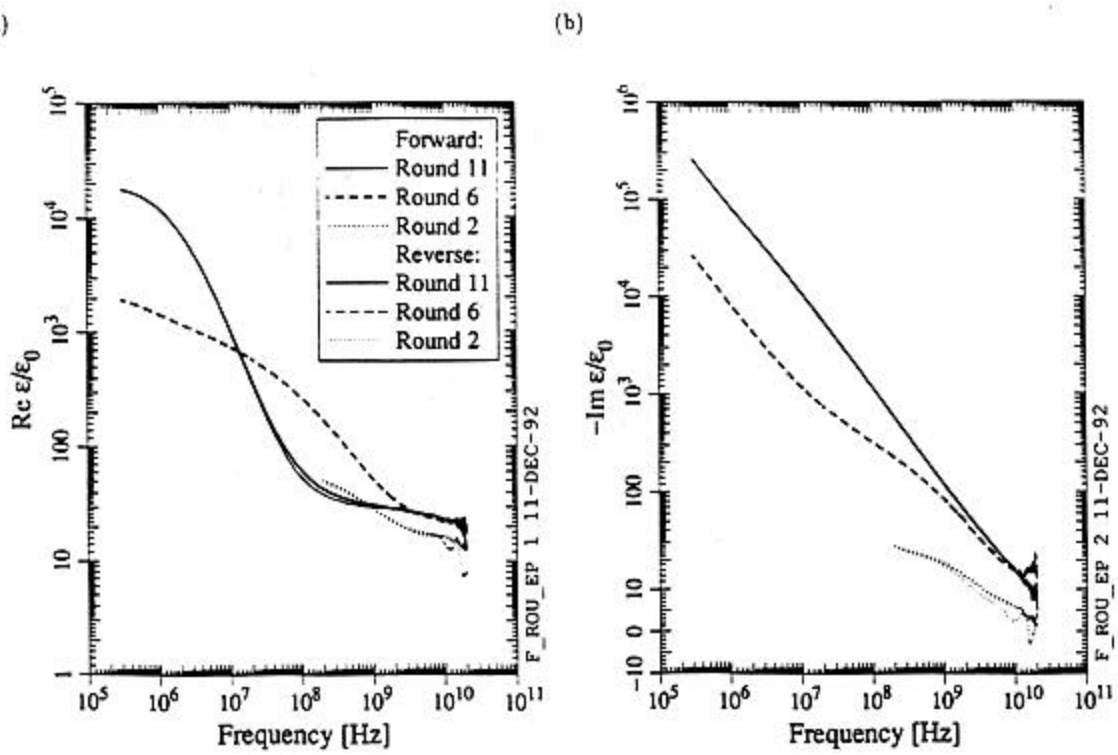

Figure 21. Comparison of the results of different rounds of measurements of (a) the real part and (b) the imaginary part (times -1) of ϵ for ferrite-50. The fit between the sample and air line was improved in round 6 and liquid metal was used in round 11.

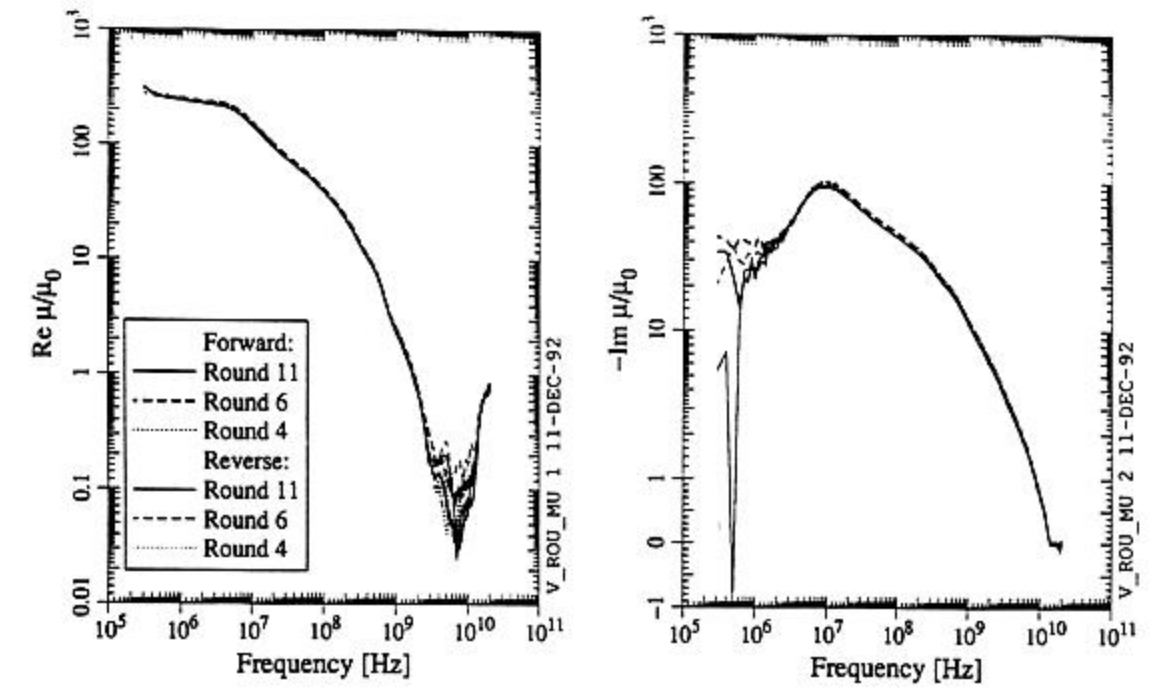

Figure 22. Comparison of the results of different rounds of measurements of (a) the real part and (b) the imaginary part (times -1) of μ for TT2-111-series ferrite. The fit between the sample and air line was improved in round 6 and liquid metal was used in round 11. TT2-111V material was used in rounds 6 and 11; another TT2-111-series ferrite was used in round 4.

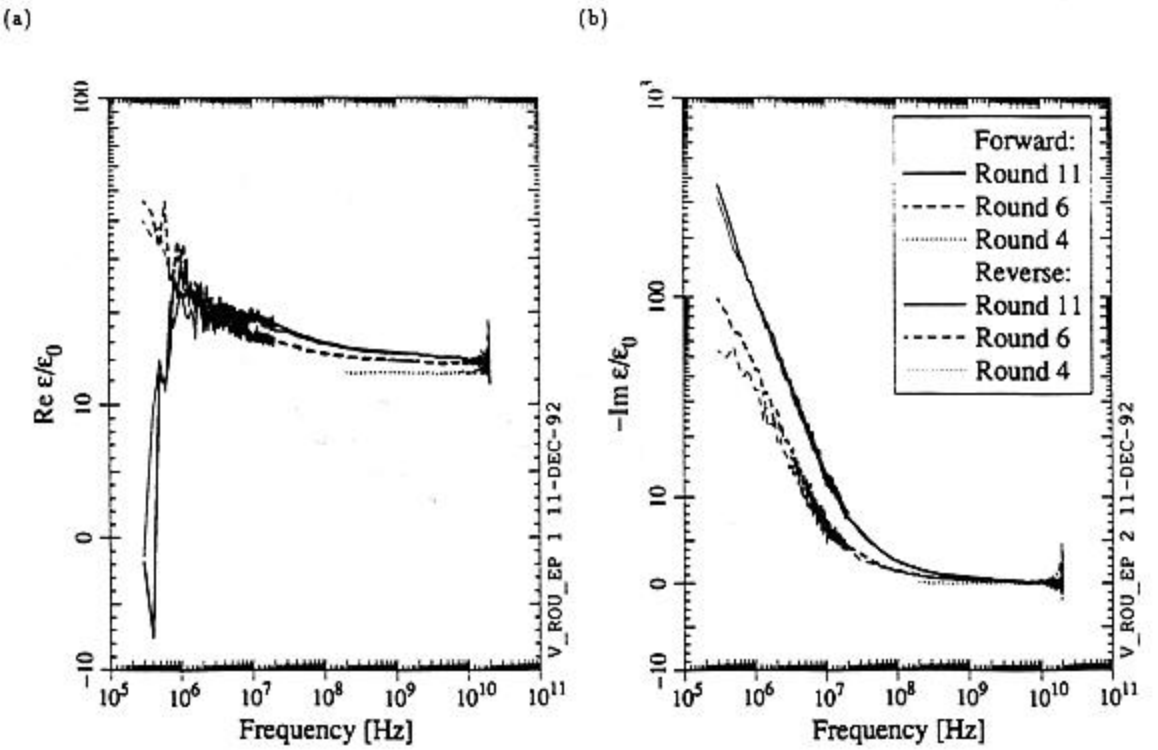

Figure 23. Comparison of the results of different rounds of measurements of (a) the real part and (b) the imaginary part (times -1) of ϵ for TT2-111-series ferrite. The fit between the sample and air line was improved in round 6 and liquid metal was used in round 11. TT2-111V material was used in rounds 6 and 11; another TT2-111-series ferrite was used in round 4.

either from variations in the actual properties of the material from sample to sample or from variations in the dimensions and surface finish of different samples. Since the faces of the sample were touched up with a hand-held grinding wheel to remove the chip from the saw cut, it is conceivable that there may be enough sample-to-sample variation to account for what we see.

6.4 Errors

The random error in the measured values of μ and ϵ would seem to be easy to estimate from the "fuzziness" in the values as a function of frequency. Aside from extreme circumstances (values close to zero, values for manganese-zinc, measurements with $d \ll \lambda_z$, *etc.*), this fuzziness is usually tolerable.

The systematic error, as usual, is more difficult to quantify. The repeated measurements discussed in the previous section allow us to make some inferences, though: (i) since a repeated measurement on the same sample was found to be significantly more reproducible than measurements on different samples, the liquid metal (when properly applied) would seem not to be the dominant source of systematic error; (ii) since measurements on different samples of the same length produce irreproducible results, it is possible that deviations in the samples from their assumed geometry are responsible for most of the systematic error. The systematic differences could be caused by variations in the microwave properties from sample to sample, though. Without being able to make reproducible results on different samples of the same length, it is difficult to draw conclusions about the systematic error in the measurement of the S-parameters.

As Don Metzger pointed out, one potential source of systematic error is via coupling to higher-order modes of propagation in the coaxial line. Since we assume only *TEM* propagation in the calculation of ϵ and μ, any coupling to other modes of propagation will produce unwanted effects. In a vacuum-filled coaxial line, the cutoff frequency of the lowest higher-order mode is evidently near 20 GHz. For a material-filled line, however, the cutoff frequency changes, usually decreasing. Actually, in an absorbing material, the distinction between cutoff and propagation cannot be made so clearly, because there is always some attenuation and some propagation. For both of these reasons, we cannot be assured that cutoff will allow us to avoid higher-order modes of propagation. However, all the higher-order modes of propagation in a coaxial line are orthogonal to the *TEM* mode, so we can hope to avoid coupling to any higher-order modes. We can also expect that deviations in the sample or air line from the ideal geometry assumed in the analysis might engender some coupling to the higher-order modes, which brings us back to the hypothesis that we can get better results by making samples of higher precision.

6.5 Ohmic Effects

Our analysis does not contain a term describing the conductivity of the material explicitly; its conductivity (if any) is lumped into Im ϵ. We can attribute Im ϵ to purely Ohmic conductivity without loss of generality. In that case, we have

$$\operatorname{Im} \epsilon = -\frac{1}{\omega \rho}, \tag{26}$$

where ρ is the resistivity of the material. In general, ρ will depend on frequency, but it may be independent of ω over some frequency range in some materials. Knowing the DC resistivity, we can predict Im ϵ from equation (26) if we assume ρ is constant.

The Im ϵ values predicted from known DC resistivities (see tables 1 and 3) are compared to measured values in figure 26. The agreement is quite close for ferrite-50 over the entire frequency spectrum. For TT2-111V, the values start to disagree significantly above 10 MHz or so. The noise in the measured values precludes a meaningful comparison for CMD10. The manganese-zinc values all disagree significantly over the measured frequency range, although they might agree in the zero-frequency limit.

7 An Alternate Analysis Procedure

We predicted large errors in μ and ϵ at frequencies where equation (18) is satisfied and saw large spikes in the measured values at those frequencies. The spikes were especially evident in low-loss materials, but also present to a lesser extent in absorbing materials. Several samples of different lengths are required in order to avoid these resonances over a broad frequency range without having problems with $d \ll \lambda_z$. The reader may wonder whether there is another way to avoid these resonances. We have found such a method that applies for materials in which either μ or ϵ is known and only one of these two quantities needs to be measured. We will now explain this method and show how it can be applied to the analysis of the dielectric measurements discussed in section 5.1.

As mentioned earlier, the spikes in μ and ϵ arise because of large errors in calculated values of Γ. This is illustrated in figure 27, which shows the measured characteristic impedance, which is calculated directly from Γ via equation (13), for the three teflon samples discussed in section 5.1. The same spikes as those we saw in μ and ϵ (figures 4 and 5) are evident. There are no corresponding spikes in the wavenumber, however, as illustrated in figure 28, which shows the measured k_z values for the teflon samples. All of the spikes seen in μ and ϵ are completely absent from the k_z values, as predicted previously. Now, in order to obtain both μ and ϵ, we need both Z and k_z; if, however, we know one of these two quantities and wish to determine only the other, we do not need both Z and k_z—either one is enough. By simply using k_z instead of Z, we can avoid the resonant errors in Z. For example, if we know μ and want to determine ϵ, we can solve for ϵ in equation (2), with the result

$$\epsilon = \frac{k_z^2}{\mu \omega^2}. \tag{27}$$

The case of knowing ϵ and wanting μ is completely analogous.

We tried the above analysis procedure on the dielectric materials, assuming $\mu = \mu_0$ and using equation (27) to obtain ϵ. Results for the three teflon samples are shown in figure 29.

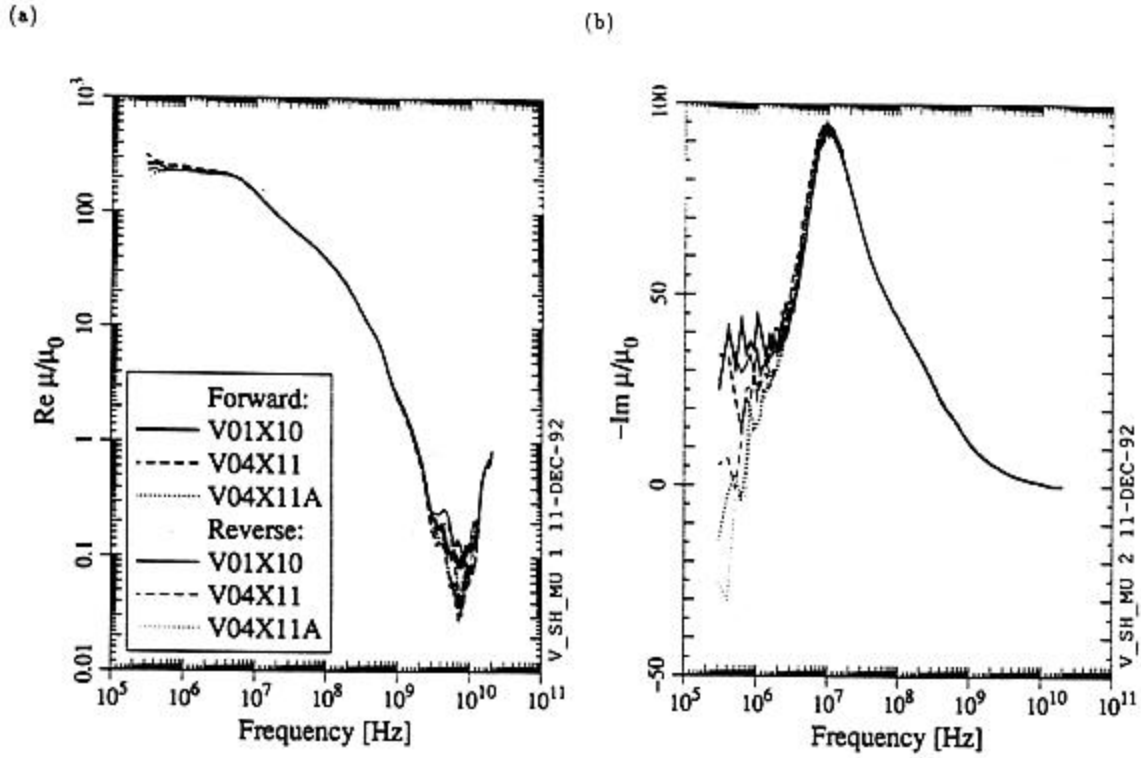

Figure 24. Comparison of the results of various measurements of (a) the real part and (b) the imaginary part (times -1) of μ for short samples of TT2-111V material. The solid lines labelled "V01X10" represent one sample; the dashed and dotted lines labelled "V04X11" and "V04X11A" represent repeated measurements on a different sample.

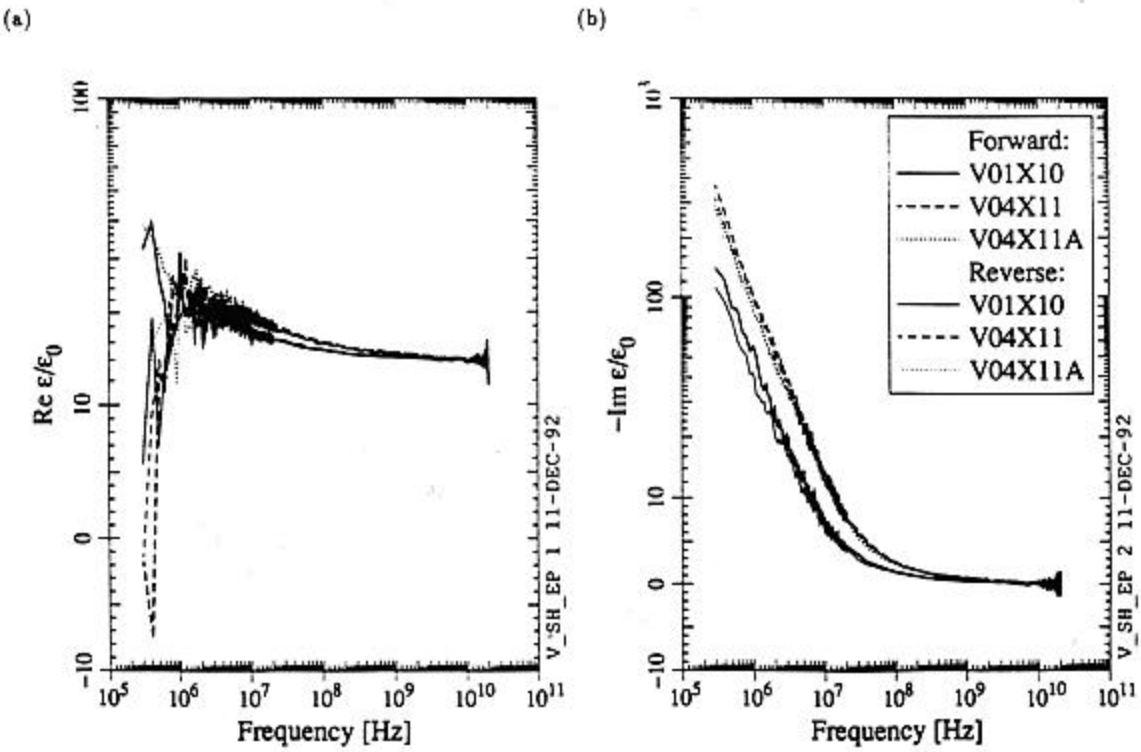

Figure 25. Comparison of the results of various measurements of (a) the real part and (b) the imaginary part (times -1) of ϵ for short samples of TT2-111V material. The solid lines labelled "V01X10" represent one sample; the dashed and dotted lines labelled "V04X11" and "V04X11A" represent repeated measurements on a different sample.

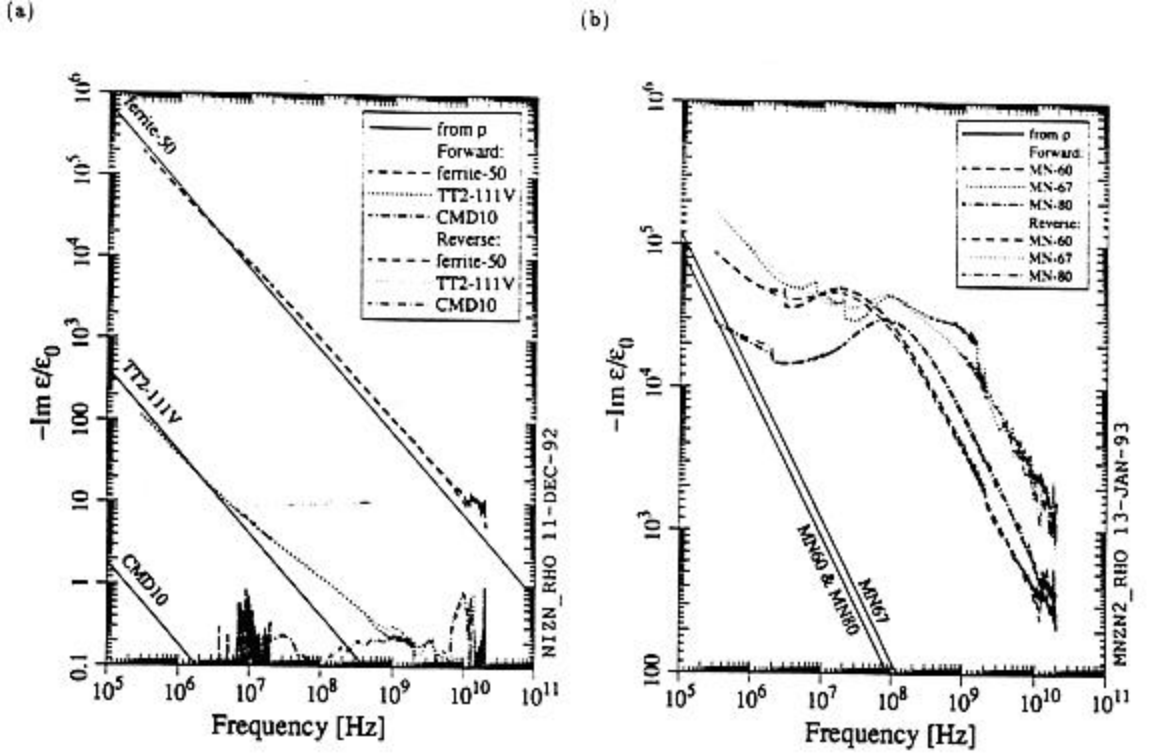

Figure 26. Comparison of measured Im ϵ values with predictions from the DC resistivity for (a) nickel-zinc ferrites and (b) manganese-zinc ferrites.

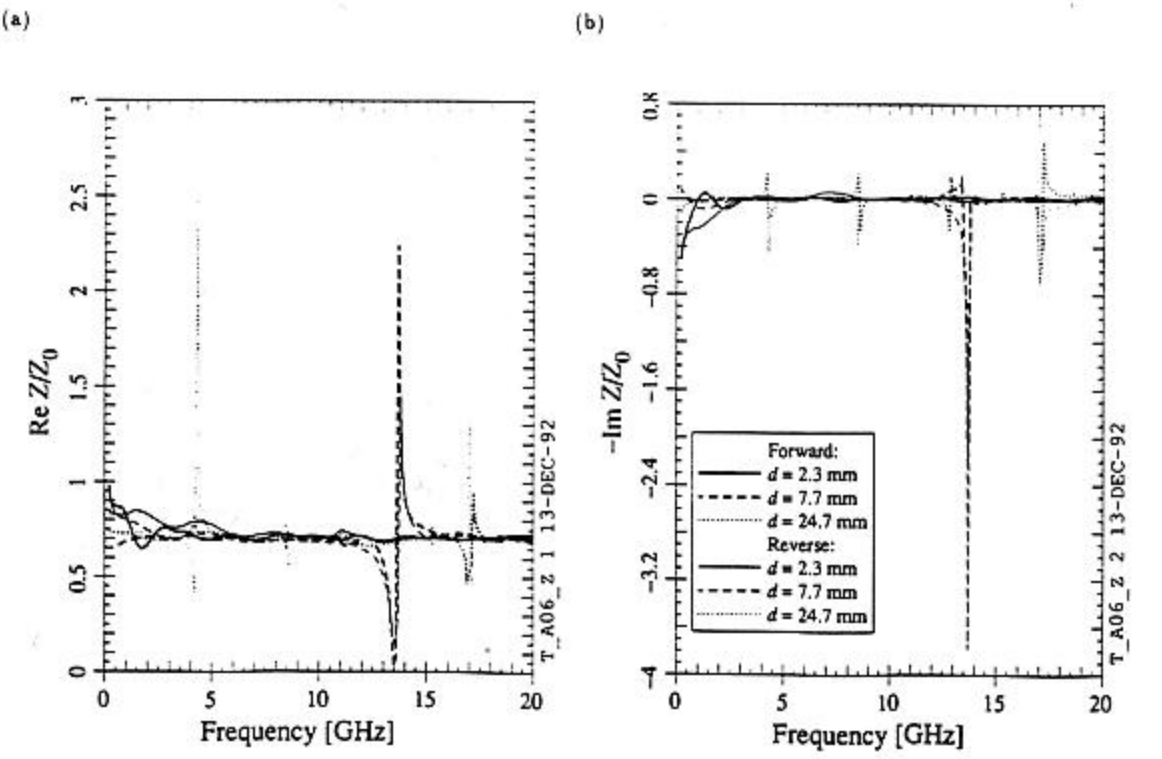

Figure 27. Measured values of (a) the real part and (b) the imaginary part (times −1) of the relative impedance for the three teflon samples.

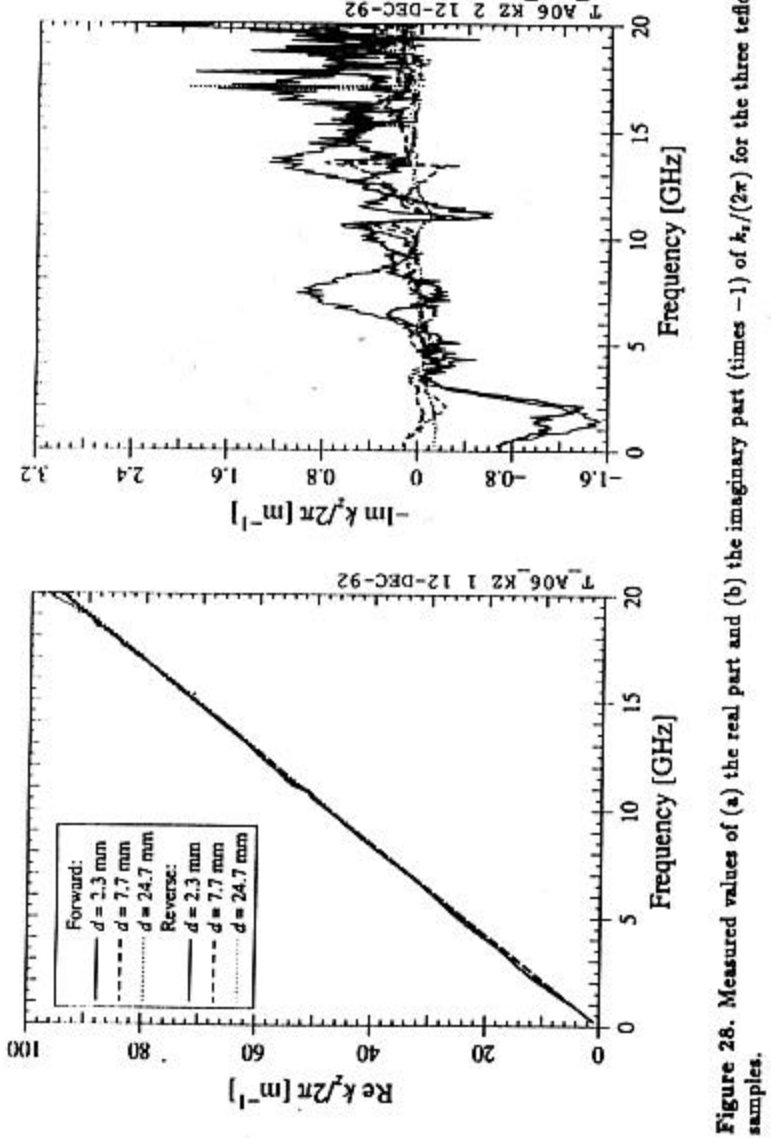

Figure 28. Measured values of (a) the real part and (b) the imaginary part (times −1) of $k_z/(2\pi)$ for the three teflon samples.

Results for air, K-7, and K-10 are shown in figure 30. As expected, the large spikes in ϵ that dominate the landscape in figures 5 and 7 have almost completely disappeared. A few traces remain, however, especially in the K-10 results. The new results also appear to be less accurate at the low-frequency end of the spectrum, as we would expect. We also expect to get the best accuracy with this method from the longest samples; this seems to be realised for our teflon samples. The results for the longest teflon sample have less error than could be obtained with any combination of the previous results for all three samples. The remarkable improvement in the ϵ values suggests that this alternate analysis method might be valuable for measurements on low-loss materials with unit permeability.

8 Conclusion

The coaxial transmission line method seems to be mostly adequate for the measurement of microwave properties of the microwave-absorbing materials we have examined, if special precautions are taken to eliminate air gaps; we cannot accurately measure real or imaginary parts of μ or ϵ that are close to zero with this method, however. The biggest problem with the measurements we have done so far is the lack of reproducibility from one sample to another. We may be able to better understand the source of this irreproducibility if we can machine the samples with better accuracy. Our results are in reasonable agreement with the results we have seen in the literature.

Acknowledgements

We would like to thank T. Tajima (KEK) and I. E. Campisi (CEBAF) for sending us samples of absorbing material. We are grateful for discussions with and suggestions from K. Akai (KEK), J. DeFord (LLNL), V. Veshcherevich (Novosibirsk), and L. Walling (SSCL). As always, we are thankful for the ideas and suggestions of our peers and for the excellent work performed by our machine shop. D. Metzger and R. Seely, in particular, deserve special mention.

References

[1] V. Veshcherevich, K. Akai, P. Barnes, W. Fox, J. Kirchgessner, D. Metzger, D. Moffat, H. Muller, H. Padamsee, J. Sears, & M. Tigner, "Higher Order Modes Damping in CESR-B Cavity," in *Proceedings of the Conference on B Factories: The State-of-the-Art in Accelerators, Detectors, and Physics* (6-10 April 1992, Stanford Linear Accelerator Center), to be published (also SRF-920701/4).

[2] W. B. Weir, "Automatic Measurement of Complex Dielectric Constant and Permeability at Microwave Frequencies," *Proceedings of the IEEE* 62, p. 33-36 (January 1974).

[3] D. Moffat, SRF/D-900306/30 (March 1991).

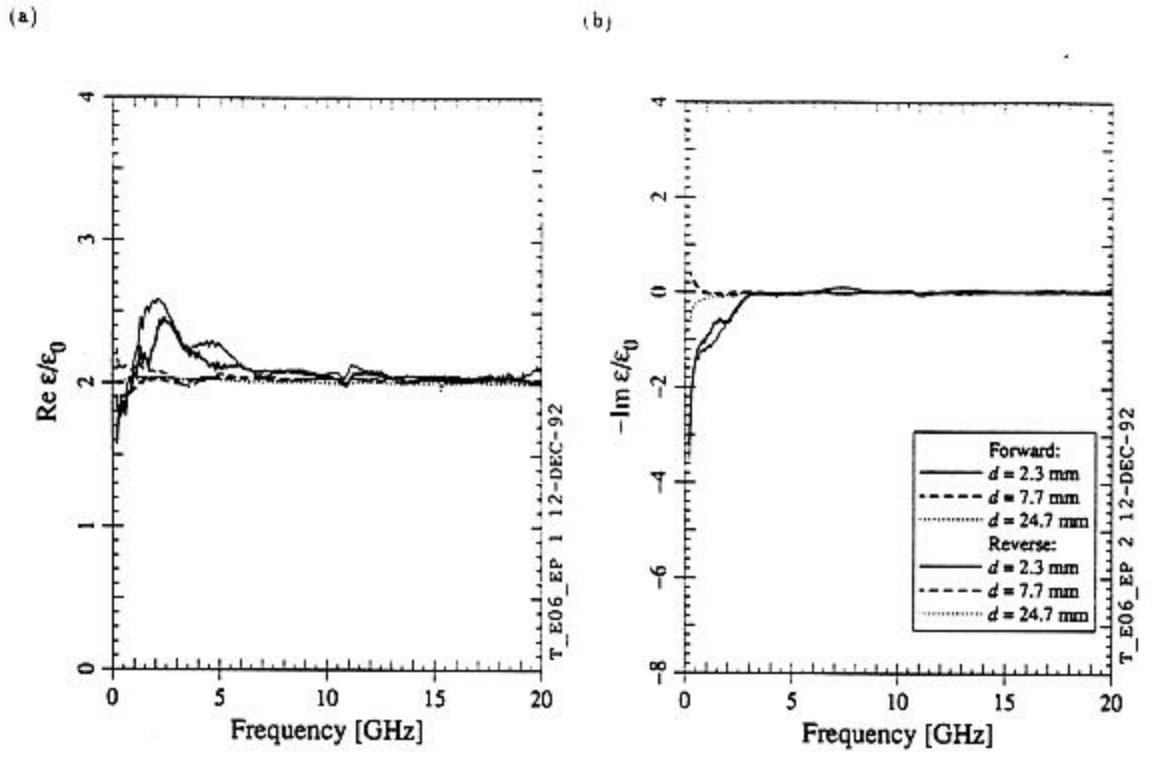

Figure 29. Measured values of (a) the real part and (b) the imaginary part (times -1) of ϵ for three teflon samples, obtained with the $\mu = \mu_0$ analysis.

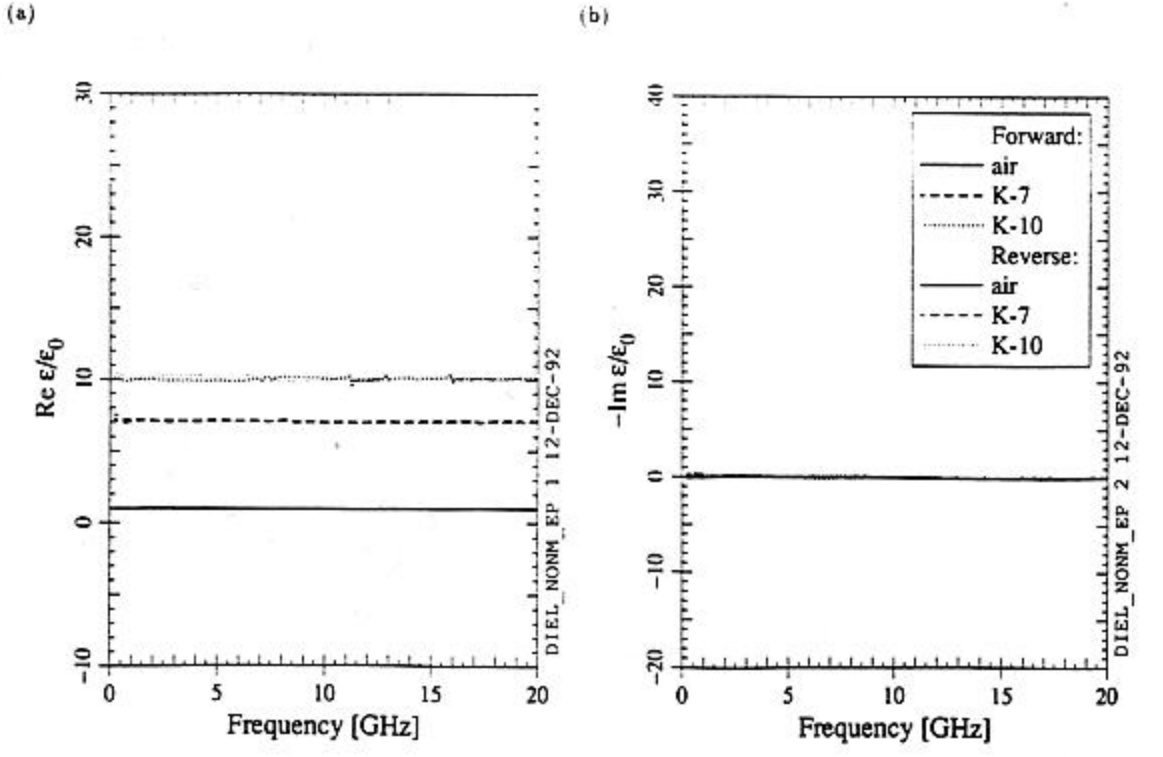

Figure 30. Measured values of (a) the real part and (b) the imaginary part (times -1) of ϵ for samples of three dielectric materials, obtained with the $\mu = \mu_0$ analysis.

[4] D. Moffat, P. Barnes, J. Kirchgessner, H. Padamsee, D. Rubin, J. Sears, & Q. Shu, "Use of Ferrite-50 to Strongly Damp Higher Order Modes," in *Conference Record of the 1991 IEEE Particle Accelerator Conference* (6-9 May 1991, San Francisco, California), L. Lizama & J. Chew, Eds., IEEE Publishing, New York, p. 664-666 (also CLNS-91/1072).

[5] H. Padamsee, P. Barnes, C. Chen, W. Hartung, J. Kirchgessner, D. Moffat, R. Ringrose, D. Rubin, Y. Samed, D. Saraniti, J. Sears, Q. S. Shu, & M. Tigner, "Design Challenges for High Current Storage Rings," in *Proceedings of the 5th Workshop on RF Superconductivity* (19-23 August 1991, DESY), D. Proch, Ed., Document DESY M-92-01, Deutsches Elektronen Synchrotron, Hamburg, Germany, April 1992, p. 138-162 (also SRF-911111-9).

[6] "Materials Measurement: Measuring the Dielectric Constant of Solids with the HP 8510 Network Analyzer," Product Note 8510-3, Hewlett-Packard, Palo Alto, California (August 1985).

[7] W. Barry, "A Broad-Band, Automated, Stripline Technique for the Simultaneous Measurement of Complex Permittivity and Permeability," *IEEE Transactions on Microwave Theory and Techniques* MTT-34, p. 80-84 (January 1986).

[8] R. M. Hutcheon, M. S. de Jong, P. Lucuta, J. E. McGregor, B. H. Smith, & F. P. Adams, "Measurements of High-Temperature RF and Microwave Properties of Selected Aluminas and Ferrites Used in Accelerators," in *Conference Record of the 1991 IEEE Particle Accelerator Conference* (6-9 May 1991, San Francisco, California), L. Lizama & J. Chew, Eds., IEEE Publishing, New York, 1991, p. 795-797.

[9] W. H. von Aulock, Ed., *Handbook of Microwave Ferrite Materials*, Academic Press, New York, 1965, p. 385-388.

[10] A. J. Baden Fuller, *Ferrites at Microwave Frequencies*, Peter Peregrinus, London, 1987.

[11] F. Caspers (CERN), private communication.

APPENDIX

The detailed results of the measurements on CMD10, IB-004, MN60, MN67, MN80, and Al-N-C are given in this appendix. All measurements were done with liquid metal present between the sample and air line; custom-made air lines were used in all cases.

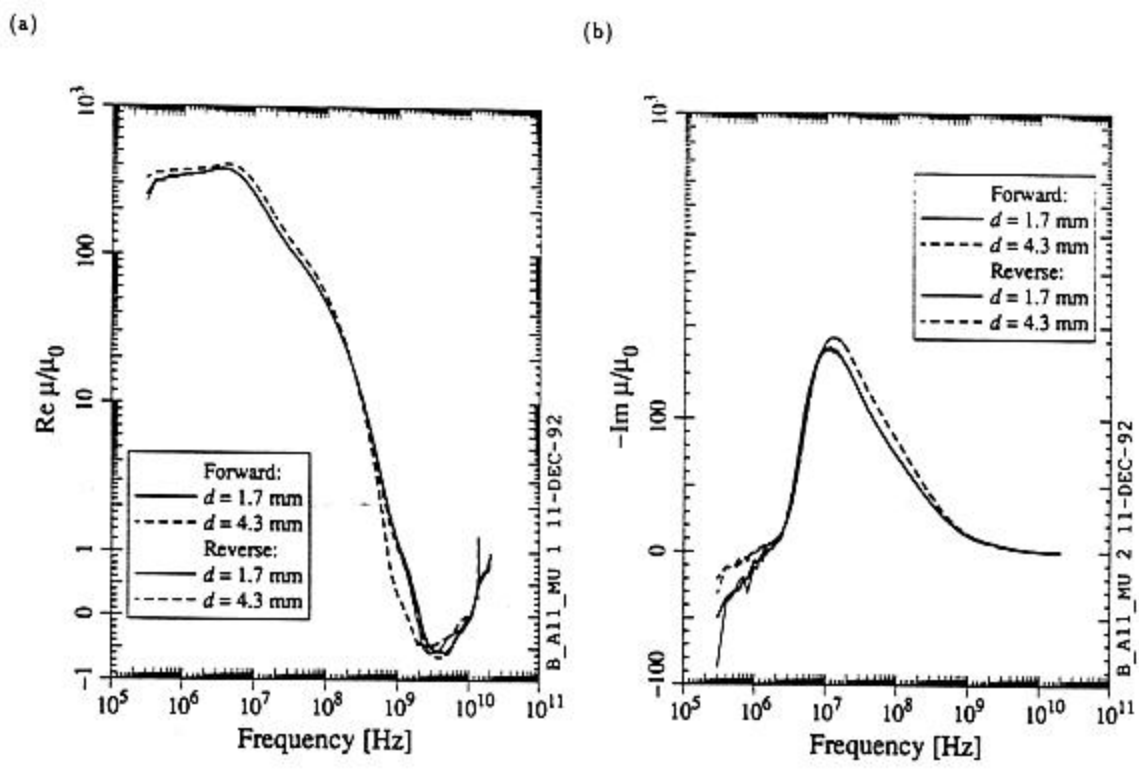

Figure 31. Measured values of (a) the real part and (b) the imaginary part (times -1) of μ for two CMD10 samples.

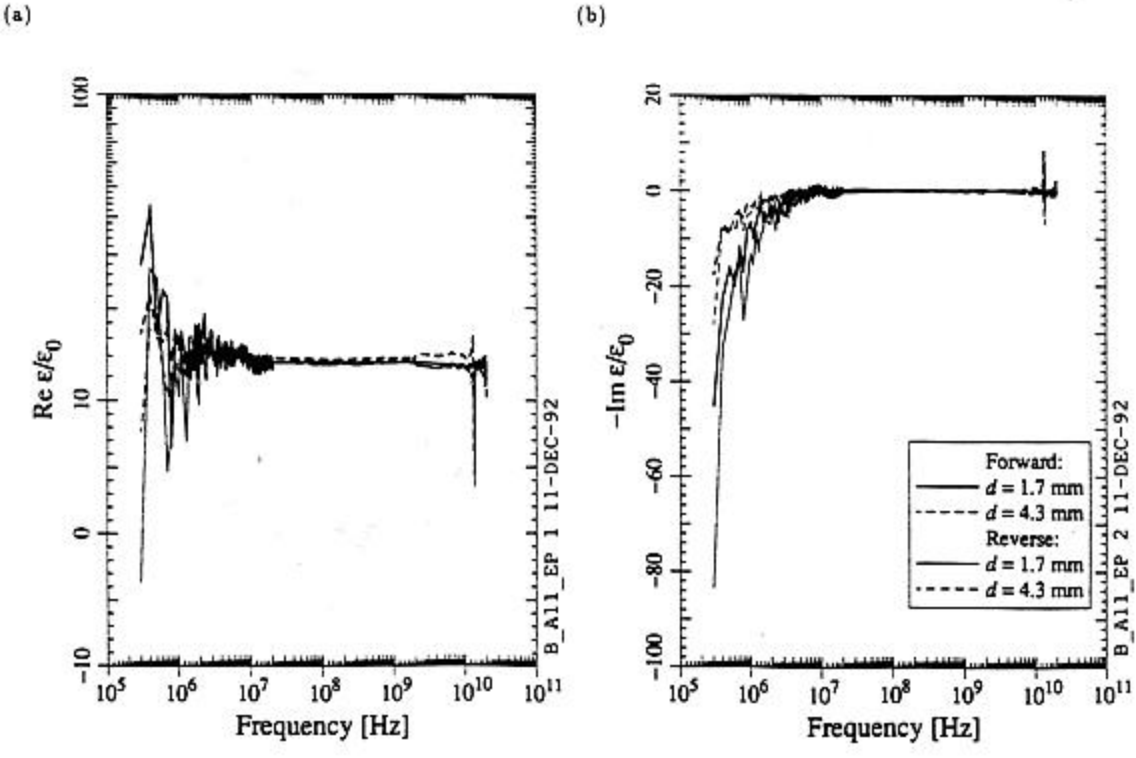

Figure 32. Measured values of (a) the real part and (b) the imaginary part (times -1) of ϵ for two CMD10 samples.

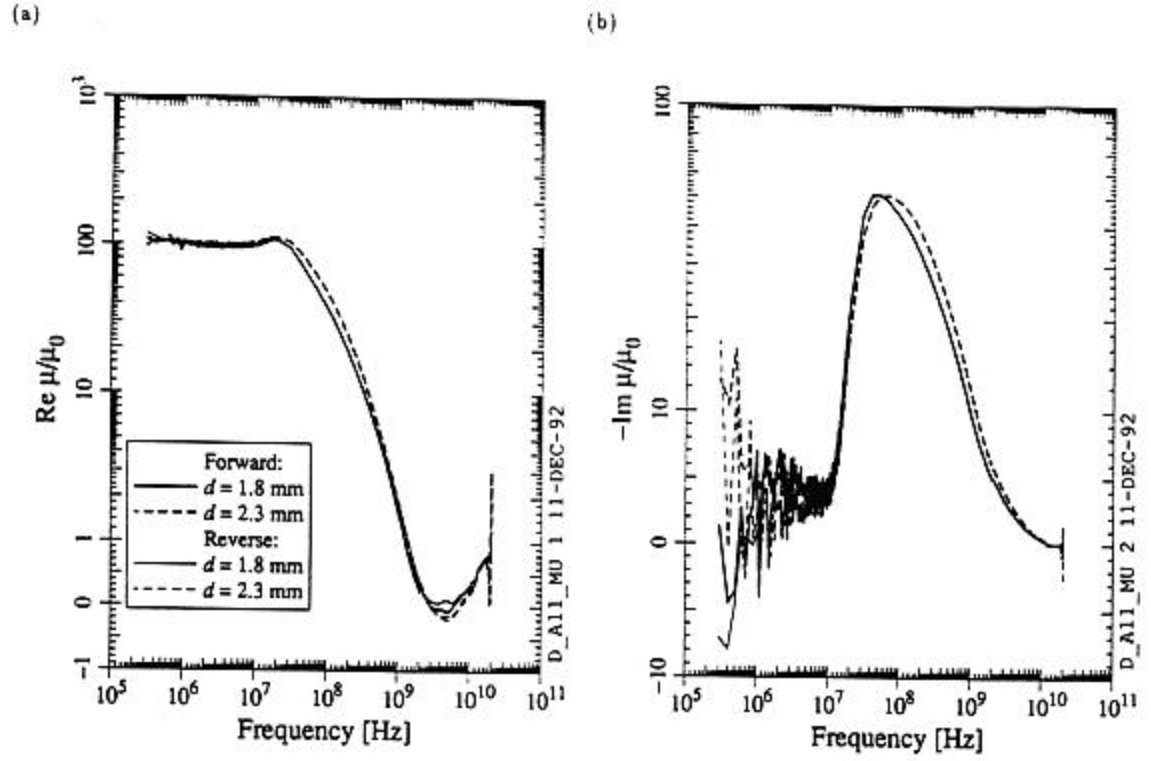

Figure 33. Measured values of (a) the real part and (b) the imaginary part (times −1) of μ for two IB-004 samples.

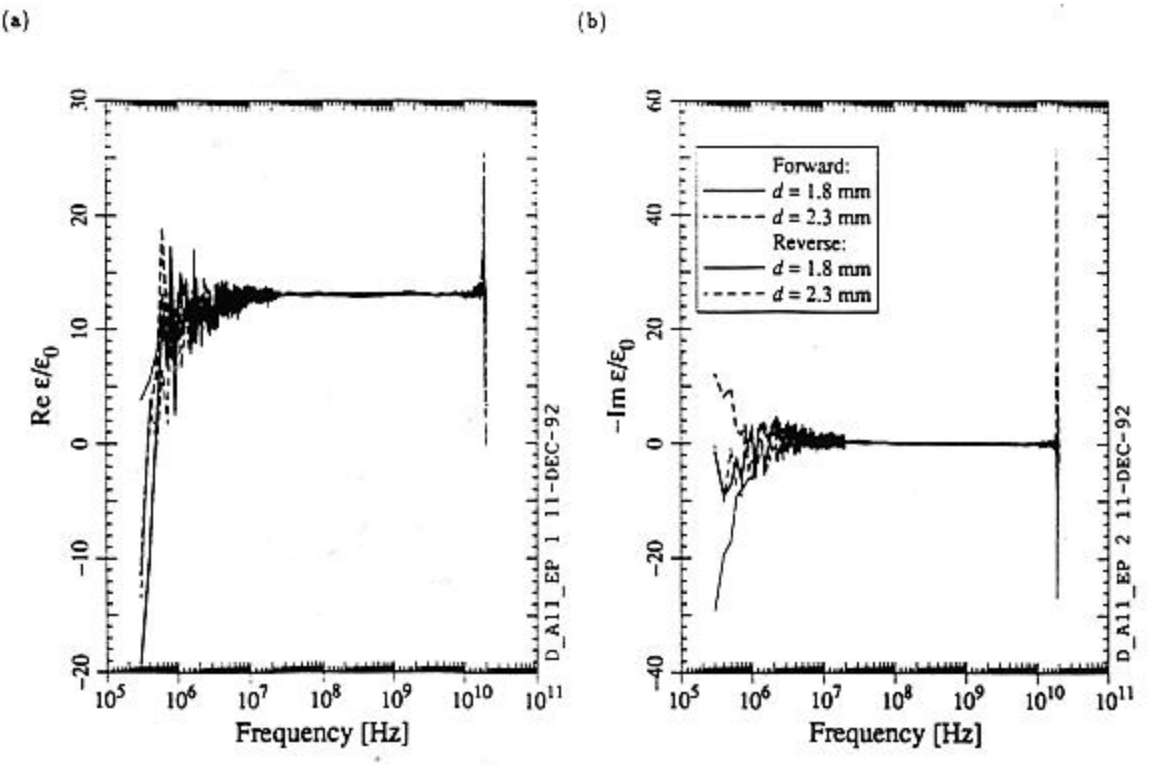

Figure 34. Measured values of (a) the real part and (b) the imaginary part (times −1) of ϵ for two IB-004 samples.

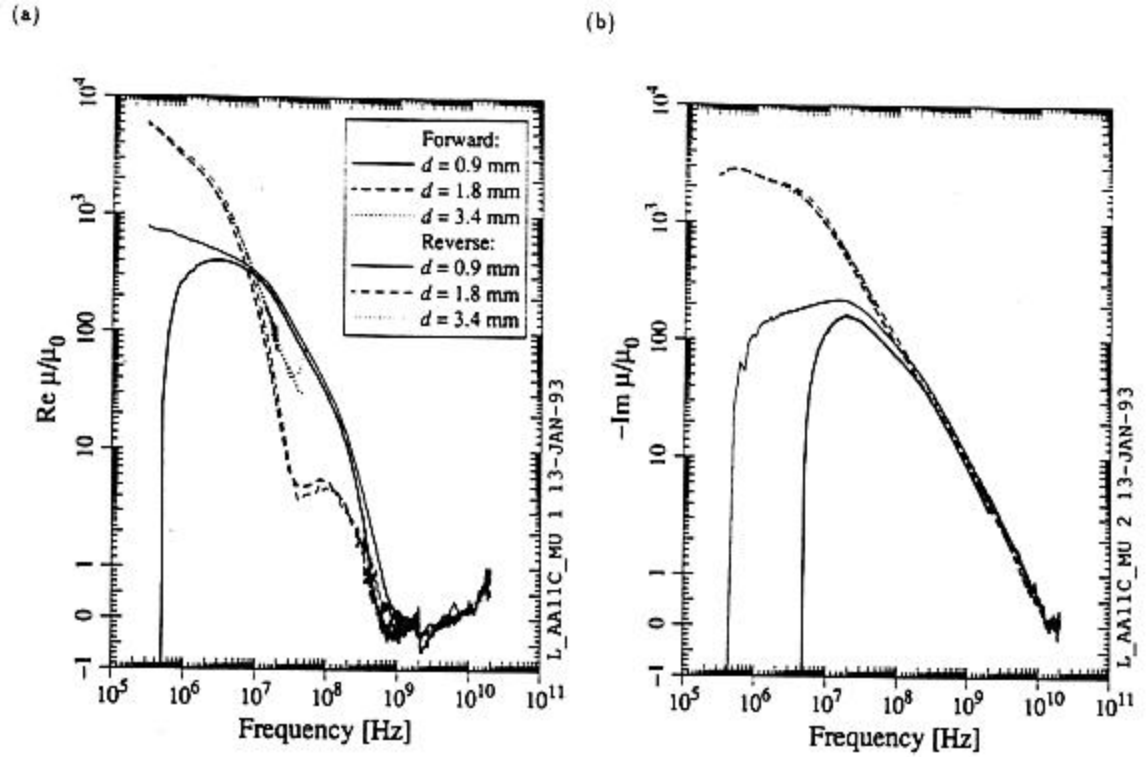

Figure 35. Measured values of (a) the real part and (b) the imaginary part (times −1) of μ for three MN60 samples. For the 3.4 mm sample, only values below 50 MHz are shown.

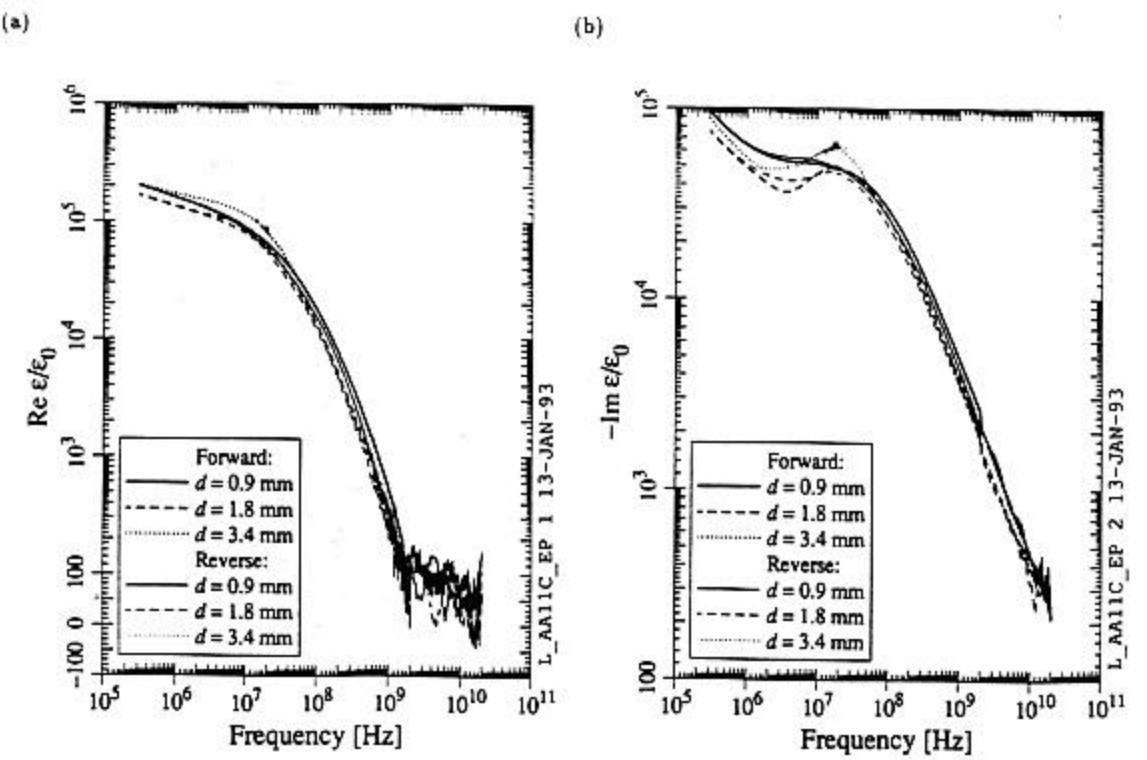

Figure 36. Measured values of (a) the real part and (b) the imaginary part (times −1) of ϵ for three MN60 samples. For the 3.4 mm sample, only values below 50 MHz are shown.

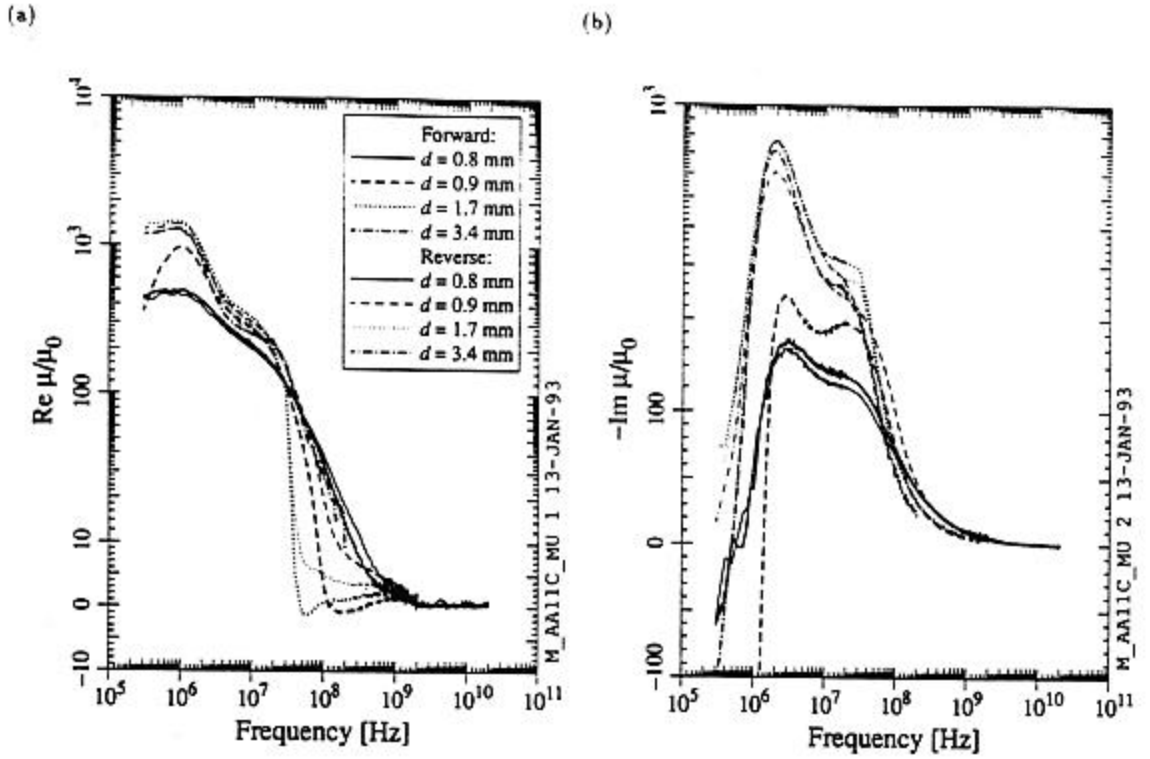

Figure 37. Measured values of (a) the real part and (b) the imaginary part (times −1) of μ for four MN67 samples. For the 0.9 mm sample, only values below 1.5 GHz are shown; For the 1.7 mm sample, only values below 800 MHz are shown; for the 3.4 mm sample, only values below 200 MHz are shown.

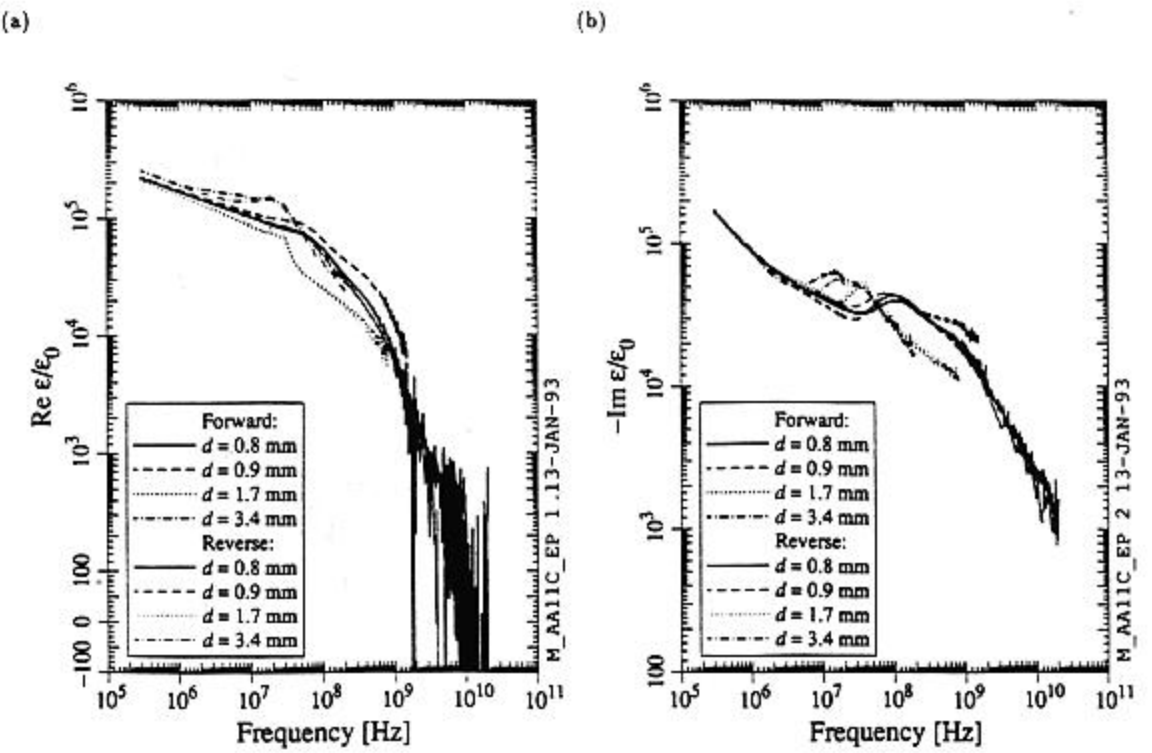

Figure 38. Measured values of (a) the real part and (b) the imaginary part (times −1) of ϵ for four MN67 samples. For the 0.9 mm sample, only values below 1.5 GHz are shown; For the 1.7 mm sample, only values below 800 MHz are shown; for the 3.4 mm sample, only values below 200 MHz are shown.

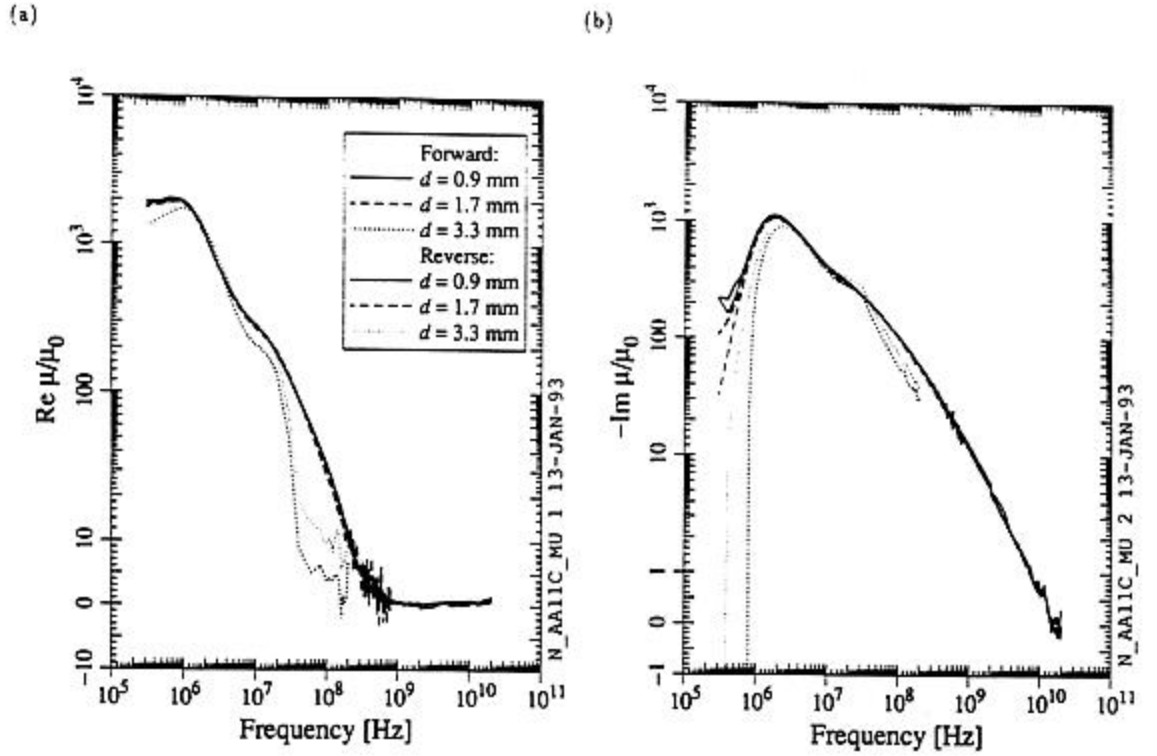

Figure 39. Measured values of (a) the real part and (b) the imaginary part (times −1) of μ for three MN80 samples. For the 1.7 mm sample, only values below 800 MHz are shown; for the 3.3 mm sample, only values below 200 MHz are shown.

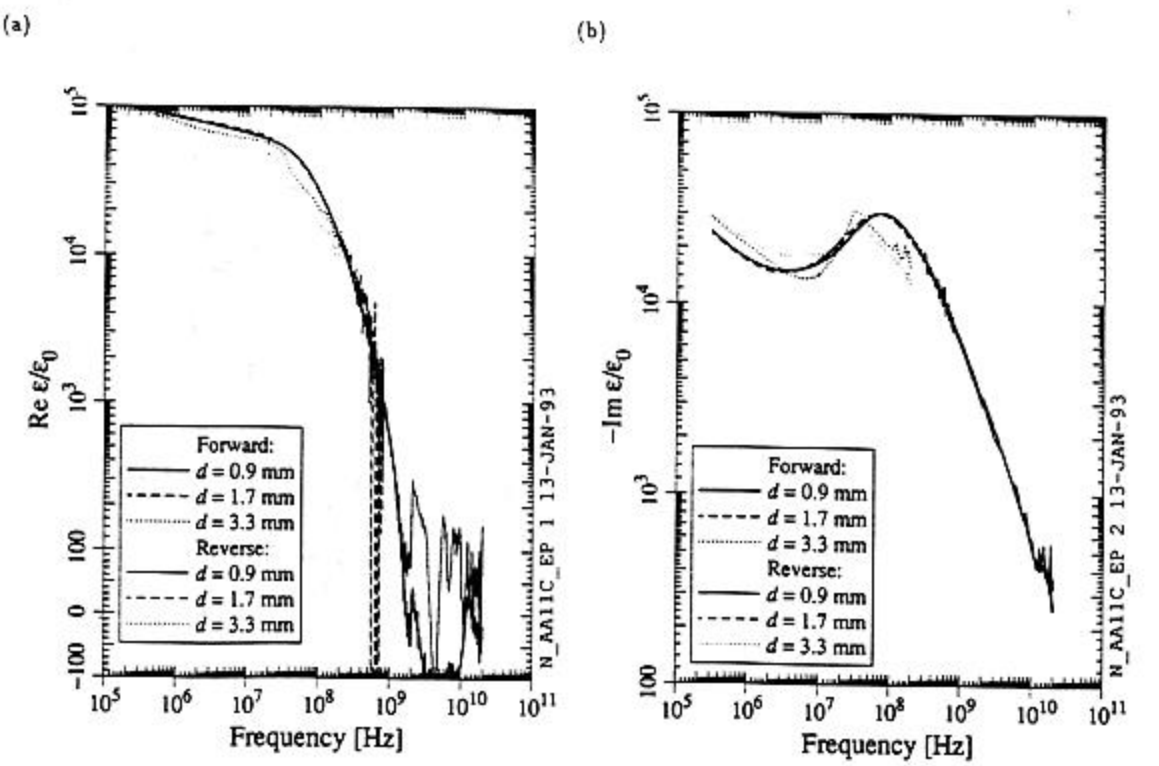

Figure 40. Measured values of (a) the real part and (b) the imaginary part (times −1) of ϵ for three MN80 samples. For the 1.7 mm sample, only values below 800 MHz are shown; for the 3.3 mm sample, only values below 200 MHz are shown.

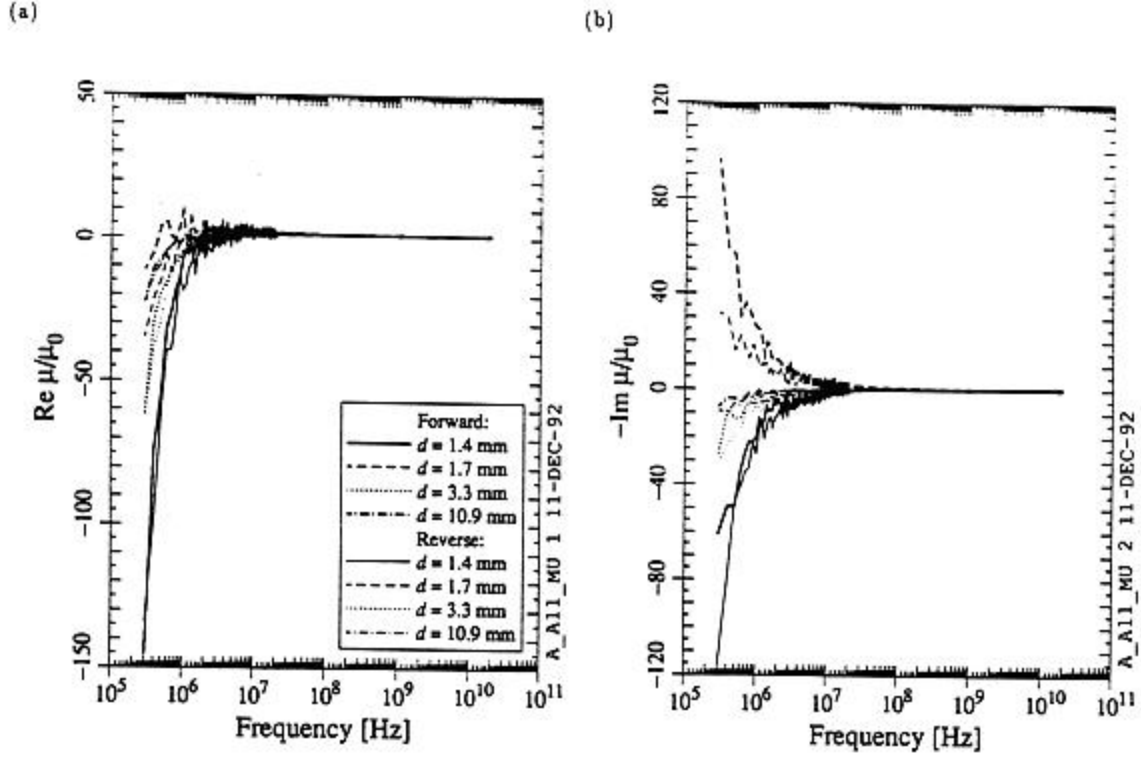

Figure 41. Measured values of (a) the real part and (b) the imaginary part (times −1) of μ for four Al-N-C samples.

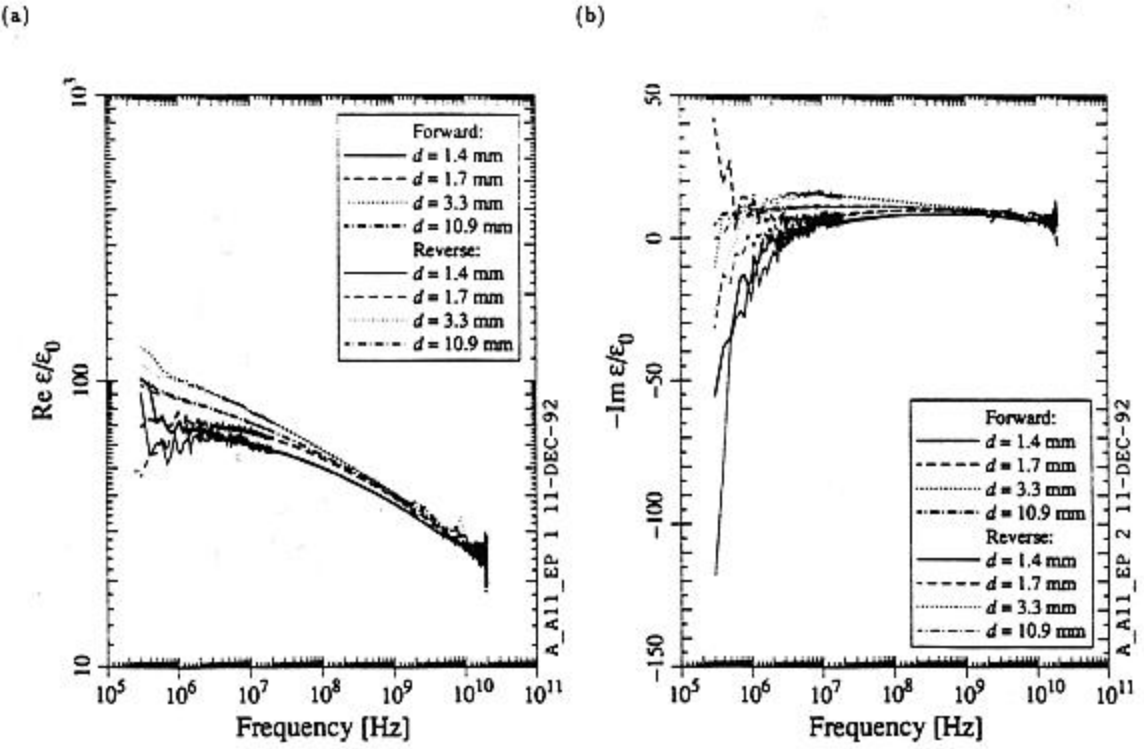

Figure 42. Measured values of (a) the real part and (b) the imaginary part (times −1) of ϵ for two Al-N-C samples.